The Polymerization with Maintaining the Primary Structure of Monomer Induced by Atmospheric Pressure Non-Equilibrium Plasma Jet

Jun Yan

Supervisor: Professor Shin-ichi Kuroda

Department of Advanced Production Science and Technology

Graduate School of Engineering

Gunma University

Aug. 2014

CONTENTS

Chapter 1 General Introduction

1.1 Plasma definition and classification

1.1.1 Thermal equilibrium plasma and non-thermal equilibrium plasma

Plasma is considered as the fourth state of matter beside solid, liquid and gas, which contains a more or less ionized gas. A commonly accepted definition is that plasma is a partially or fully ionized gas. From a macroscopic point of view, plasma is electrically neutral. And in the universe most of the observable matter (more than 97%) is in the plasma state. However, plasma is electrically conductive and a lot of free charge carriers are contained in it [1].

The properties of the plasma change in terms of electron density and electron temperature depending on the amounts of energy transferred to the plasma. Plasma was distinguished into different categories by two parameters (see Fig. 1-1) [2]. Generally, plasmas are divided into two categories (see Fig. 1-2), *i.e.* thermal equilibrium plasma (thermal plasma) and non-thermal equilibrium plasma (cold plasma). In thermal plasma, transitions and chemical reactions are controlled by collisions and not by radiative processes. Moreover, collision phenomena are micro-reversible in thermal plasma, suggesting that each kind of collision is balanced by its inverse (excitation/de-excitation; ionization/recombination; kinetic balance) [3]. Therefore, in thermal plasma on the basis of the temperature of heavy particles, the electron temperature is equal to the gas temperature [2].

From Fig. 1-2, it is easily seen that non-thermal equilibrium plasma (cold plasma) should be described by two temperatures: electron temperature (T_e) and heavy particle temperature (T_h) [3]. Because of the huge mass difference between electrons and heavy particles, the plasma temperature (or gas temperature) is determined by T_h. On the other hand, the electron-induced

de-excitation rate of the atom is generally lower than the corresponding electron-induced

excitation rate because of a significant radiation de-excitation rate [4]. Therefore, the density

distribution of excited atoms in cold plasma is possible to depart from Boltzmann distribution,

suggesting that the gas temperature is much lower than the electron temperature [5-7].

1.1.2　Atmospheric pressure non-equilibrium plasma

Fig. 1-2 shows effect of gas pressure on electron temperature (T_e) and gas temperature (T_g)

[3]. It can be clearly seen that at a lower pressure ($10^{-4} \sim 10^{-2}$ kPa) the gas temperature is much

lower than the electron temperature. The heavy particles are excited or ionized through inelastic

collisions with electrons. These inelastic collisions do not raise the temperature of heavy particles.

However, collisions in the plasma intensify when the gas pressure becomes higher. They lead to

both plasma chemistry (by inelastic collisions) and heavy particles heating (by elastic collisions).

Then, the difference between T_e and T_g decreases; plasma state is close to the thermal equilibrium

state. How to prevent heavy particles from being heated is crucial to generate non-thermal

equilibrium plasma at atmospheric pressure. It was found that the density of the feeding power

affects the plasma state (thermal equilibrium or not) at a large extent. Namely, a high power

density lead to atmospheric pressure thermal equilibrium plasma (e.g. arc plasma); a low density

of feeding power or a pulsed power supply lead to atmospheric pressure non-thermal equilibrium

plasma.

1.2　Comparison between vacuum plasma polymerization and atmospheric pressure plasma polymerization

From the 1960s and 1970s, plasma polymerization was considered as a method of

polymerization [8-17]. Although some important differences in polymer formation mechanisms

and the properties of resultant polymers were recognized, the underlying concept was an extension

of the concepts of polymerization and polymers developed with conventional polymers [14].

Consequently, the underlying concept was represented, for example, by the preparation of a thin

layer of polystyrene by the plasma polymerization of styrene or the preparation of a thin layer of

polytetrafluoroethylene by the plasma polymerization of tetrafluoroethylene. In other words,

plasma polymerization was regarded as a new and unique method of polymerization.

1.2.1   Vacuum plasma polymerization

Because most plasma polymerization was carried out in a vacuum, it is important to review

the polymerization that occurs in a vacuum system.

First, in the vacuum system number of molecules is very lack. For example, one mole of

styrene (molecular weight 100 g/mol) occupies ~0.1 liters as a liquid. When 1 mol of styrene is

vaporized, it occupies 22.4 liters under 1 atm pressure and at 0 ℃. Therefore, in a hypothetical

situation, styrene vapor under 1 atm contained in the same volume (i.e., 0.1liter) contains $1/22.4 =$

4.5×10^{-3} times fewer molecules than the liquid in the same volume. When the system pressure is

reduced to 0.133 kPa, this rate is further reduced to 6.0×10^{-6}. In other words, in a vacuum, by

definition, not many molecules are available. Therefore, polymerization in a vacuum involves the

formation of polymers from very sparsely dispersed monomers.

Second, changing of the ceiling temperature of polymerization is as a function of pressure.

Because of the very small number of molecules available in a vacuum, the relatively slow

polymerization process based on the step-growth polymerization of molecules (not reactive

species) fails to explain the rather rapid formation of polymers that is found in plasma

polymerization.   Therefore,   the   relatively   slow   polymerization   based   on   step-growth

polymerization can be categorically eliminated from the consideration of polymer formation in a vacuum. Then, chain propagation should be examined as a possible practical mechanism of polymerization.

Low-pressure plasma discharge are widely used in materials processing, because they have a number of distinct advantage: 1) low breakdown voltage; 2) a stable operating window between spark ignition and arcing; 3) an electron temperature capable of dissociating molecules (1-5 eV), but a low neutral temperature; 4) relatively high concentration of ions and radicals to drive etching and deposition reactions [18].

Short plasma pulses (a few μs) can activate vinyl- or acrylic monomer molecules, produce radicals, and initiate the plasma polymerization reaction, which is expect to consist of more chemically-regular products than those encountered in the continuous-wave (cw) counterpart, where predominantly random radical recombination occurs [19].

Ideally, pulse-on/pulse-off ratio will decide the composition of the plasma polymer. But it is note that all of the pulsed plasma polymerization processes have very low deposition rates.

1.2.2 Atmospheric pressure plasma polymerization

But the cost of the vacuum equipment is too high and the strict of object by the vacuum plasma, the atmospheric pressure plasma polymerization becomes of interest since they may be adapted to large substrates that are manufactured in a continuous fashion [20-26].

Kurosawa et al. [27-29] had developed micro-discharge for micro-plasma polymerization, which are obtained by a very high frequency (438 MHz) micro-plasma jet machine at atmospheric pressure (in a thin quartz capillary, 1.5 mm in diameter). They used the micro-discharge for the local synthesis of very thin plasma polymerized-PS coatings for bio-sensors and chemical-sensors

applications.

By using plasma gases (noble gas like He, Ar, or N_2, or air), it is possible to obtain glow and filamentary discharge at atmospheric pressure. The homogeneity of the He discharge is due to the existence of its high energy metastables (19.82 eV for 2^3S and 20.62 eV for 2^1S) [30, 31].

For other applications, argon is an alternative of choice, as it also possesses high-energy metastable states (11.55 eV for $^3P_2$ and 11.72 eV for $^3P_0$) [32]. Argon metastable has a shorter lifetime than helium, but the availability of argon makes it much more interesting for industrial application [33]. And the existence of neutral metastable states is of huge importance for the homogeneity of the discharge. Moreover the major difference between the deposition mechanisms of coatings at atmospheric pressure and those at low pressure is depend on the existence of metastables, and the presence of other excited species of the plasma gas, which the metastables and the other excited species can collide with precursor molecules, to initiate the polymerization and growth mechanisms, such as electrons are doing at low pressure [3].

The proportion of additives plays an important role because it controls the density of metastable species at the time of discharge ignition. Oxygen (like N_2) disturbs the discharge by quenching the He metastables which stabilize the discharge, which contributes to render the discharge more homogeneous [30].

Kasih et al. [34] has succeeded in polymerizing methyl methacrylate (MMA) with keeping the primary structure of MMA with using an atmospheric pressure non-equilibrium argon (Ar) plasma jet very recently, which is considering of the effect of Ar metastable atom to the MMA.

The plasma polymerization process that takes place at atmospheric pressure is usually considered as being almost similar to the one proposed by Yasuda for low pressure plasmas [14].

1.3 Operational parameters of plasma polymerization

Plasma polymerization is highly system-dependent, meaning results depend on the reactor and operational conditions. The major factor that causes system dependency is the design factor of the reactor that indicates the operational conditions to be used. Because of this, two important aspects of plasma polymerization are discussed below.

1.3.1 Voltage input of plasma polymerization

In order to understand the nature of atmospheric pressure non-equilibrium plasma discharge, the important discharge parameters (such as discharge voltage, discharge current, transferred charge etc.) must be characterized. Generally, the impedance of the entire load and not just of the discharge was measured electrically.

An equivalent electric circuit can be used to characterize the overall discharge behavior. An example of such a circuit is shown in Fig. 1-3 [38]. In this case, one side dielectric barrier discharge is employed. As long as the gap voltage (U_g) is smaller than the ignition voltage (breakdown voltage), there is no discharge and the plasma device acts as a series combination of two capacitances: the gap capacitance (C_g) and the capacitance (C_d) representing the dielectric. Then the total capacitance C is given by the expression:

$$C = \frac{C_d C_g}{C_d + C_g} = \frac{C_g}{1 + C_g/C_d} = \frac{C_g}{1 + d/(\varepsilon_r g)}$$

（1-1）

Since typically ε_r= 5 - 10 (glass dielectrics) and $g \approx d$ (for the operation condition of barrier discharge, gap distance g is variety between 0.2 - 5 mm, and the thickness d is between 0.5 - 2 mm), the term $C_g / C_d = d / (\varepsilon_r g) \approx U_d / U_g \ll 1$ (U_d represents the voltage across dielectric barrier). Therefore, the total capacitance (C) mainly depends on the capacitance of the gas gap (C_g). The gap voltage (U_g) is close to the feeding voltage. If U_g reaches the ignition voltage,

micro-discharges are initiated. Within every half cycle, the discharge voltage remains approximately constant, although the current flow through discharge gap is maintained by a large number of micro-discharges. Figure 1-4 shows a general setup for electrical measurement of DBD (Dielectric Barrier Discharge) for estimating the parameters [38]. Capacitance C represents the DBD fed by an alternating voltage $U(t)$. The charge-voltage characteristic (Q - U) and the current pulse shape $I(t)$ can be registered alternatively using either a resistance R_d ($R \approx 50\ \Omega$) or a capacitance C_d ($C \approx 10$ nF) by using an oscilloscope. The applied high voltage is measured by a high-voltage probe. Using this measurement set up, the important electric operation parameters of DBDs, such as discharge voltage and discharge current can be measured. The discharge voltage (U_D) can be calculated by the following expression [38]. It is close to the measured voltage (U_{min}) since $C_g / C_d = d / (\varepsilon_r g) \approx U_d / U_g \ll 1$.

$$U_D = U_{min} \frac{1}{1 + C_g/C_d} \tag{1-2}$$

The dissipated electric energy consumed per voltage cycle (E_{el}) can be measured by the Lissajous figure (see Fig. 1-5) [9, 33].

$$E_{el} = \int U(t)dQ = C_{meas} \int U(t)dU_{meas} = 4C_d \frac{1}{1 + C_g/C_d} U_{min}(U_{max} - U_{min}) \tag{1-3}$$

Obviously, the dissipated electric energy consumed per voltage cycle (E_{el}) is equal to the area of Q-U diagram shown in Fig. 1-5. Then, the dissipated electric power (consumed electric energy) can be estimated by the following expression:

$$P = \frac{1}{T} E_{el} = fE_{el} \tag{1-4}$$

The number of micro-discharge series per half cycle ($N_{T/2}$) can be derived under the assumption that all series transfer an identical charge ΔQ by the following expression.

$$N_{T/2} \approx \frac{2C_d}{\Delta Q}\left(U_{max} - U_{min}\right) \hspace{4cm} (1\text{-}5)$$

Assuming that all micro-discharges of one series (causing one single current pulse) have nearly identical properties, then $\Delta Q \approx nq$, where n is the number of micro-discharges in a series and q is the charge transferred by one single micro-discharge. The quantity of charge transfer is mainly determined by the categories of dielectric and the width of gap spacing [38].

1.3.2 Monomer flow rate of plasma polymerization

Although there are numerous reports on the deposition rate of plasma polymerization as a function of some of the operational parameters, relatively little is known about how properties of plasma polymer depend on the operational parameters.

In the tail flame portion of glow discharge used in a series of studies, as reported in the report [35], the flow rate is well defined and the deposition rate is uniquely related to the flow rate.

Studies by Yasuda et al. [36] showed that properties (free-radical concentration, gas permeability, internal stress, and contact angle of water) of plasma polymers of acetylene and of acrylonitrile were related to the flow rate of monomer in an electrodeless glow discharge. They found that the monomer flow rate has a strong influence on free-radical concentration, gas permeability, and internal stress but little influence on the contact angle of water.

Kobayashi et al. [37] discussed the effects of flow rate on the plasma polymerization of ethylene in an RF discharge using both a tubular and a bell-jar-type of reactor. The work showed that monomer flow rate and the inlet flow configuration have a strong influence on both the rate of polymer deposition and the uniformity of the deposited film. And, they also found that at low flow rates the polymer thickness decreased in the flow direction, while at high flow rates the polymer thickness increased.

1.4　Objectives of this study

As mentioned above, atmospheric pressure non-equilibrium plasma polymerization is a beneficial technology due to its low cost and flexibility in terms of its operation [39-47]. So far, though a variety of polymerization have been developed into a capillary micro-channel, the polymerization mechanisms induced by the atmospheric pressure plasma are not clear yet, especially about the method how to maintain the monomer primary structure [48-61]. On the other hand, it will be cleared if we find experimental conditions required for keeping the monomer structure to illuminate the polymerization mechanism in the atmospheric pressure plasma.

In this point of view, it should be remarked that we have succeeded in maintaining the monomer structure through the plasma polymerization of MMA with using argon (Ar) plasma jet [34]. This device has been commercialized under the name of "CAPPLAT" by Cresur Corporation of Japan. Thus this thesis aims to clarify the necessary conditions for the polymerization with maintaining the primary structure of monomer induced by the atmospheric pressure non-equilibrium Ar plasma jet as well as to interpret the polymerization mechanism by taking the metastable Ar (Ar^m) into account.

In Chapter 2, the polymerization of MMA was carried out by means of an atmospheric pressure non-equilibrium helium (He) plasma jet. The polymerization using Ar plasma under the same condition was also performed for comparison following Kasih's investigation. The obtained results showed that Ar plasma can polymerize MMA more efficiently than He plasma not only in terms of polymerization rate but also polymer composition. The polymerized MMA by He plasma was recognized to have more disordered structure judging from its broadened C-O-C absorption in Fourier transform infrared (FT-IR) spectrum. This observation brought a working hypothesis that a

monomer of which ionization potential is close to or larger than the energy of metastable atom in plasma can be polymerized easily with retaining the primary structure. This working hypothesis was supported by the fact that styrene of which ionization potential is as small as 8.50 eV, much lower than Arm energy, was hardly polymerized by Ar plasma.

In Chapter 3, in order to ascertain the working hypothesis postulated in the former chapter, a non-equilibrium atmospheric pressure plasma was applied for the polymerization of the methacrylic monomers such as (2-hydroxyethyl methacrylate (HEMA), methacrylic acid (MAA) and butyl methacrylate (BMA)). These monomers were selected on the basis of their energy levels of the highest occupied molecular orbital (HOMO) calculated using the PM3 method. It was shown that the selected monomers were successfully polymerized with retaining the functional groups of ester or acid. The polymerization mechanism was discussed on the basis of the optical emission spectroscopy (OES) of the plasma. The Stern-Volmer plot to express the dependency of emission intensity of Ar plasma jet on the monomer concentration became linear indicating that the energy transfer form Arm to the monomer took place quantitatively. It was strongly suggested that the functional groups composed of monomer could be retained when the polymerization was proceeded for the monomer of which ionization potential is close to the energy of Ar^m.

In Chapter 4, the non-equilibrium atmospheric pressure Ar plasma was applied to the polymerization of maleic anhydride (MA). Since the ionization energy of MA is 10.5 eV that is close to the energy of Ar^m, the polymerization mechanism assumed in the former chapters suggested it possible for MA to be polymerized. The deposited films were analyzed by using Fourier transform infrared spectroscopy (FT-IR) proving the monomer was successfully polymerized with retaining the functional groups. The intensity of optical emission spectroscopy

(OES) of the plasma jet was found to become weaker when the monomer was introduced into the jet. This was interpreted as the result of the energy transfer from Ar^m to the monomer. It was suggested that the excited MA changed into π-π^* transition state to produce dimer biradicals which initiated the polymerization. As it has been assumed that MA polymerizes with much difficulty because of high steric hindrance resulting from disubstitution and only a few exceptional reports have appeared concerning the photo-homopolymerization of MA, the procedure invented in the present study is a promising practical method for the production of homopolymeric materials of MA.

References

[1] C. Tendero, C. Tixier, P. Tristant, Spectrochimica Acta, Part B 61, 2 (2006).

[2] M. I. Boulos, P. Fauchais, E. Pfender, Thermal Plasmas: Fundamental and Applications. Volume I, Plenum Press, New York, ISBN: 0-306-44607-3, 452 (1994).

[3] D. Merche, N. Vandencasteele, F. Reniers, Thin Solid Films, 520, 4219-4236, (2012).

[4] R. H. Huddlestone, S. L. Leonard, Plasma Diagnostic Techniques, Academic Press, New York, (1965).

[5] H. R. Griem, Plasma Spectroscopy, McGraw-Hill, New York (1964).

[6] W. Lochte-Holtgreven, Plasma Diagnostics, North-Holland, Amsterdam (1968).

[7] M. Mitchner, C. H. Kruger, Partially Ionized Gases, Wiley, New York (1973).

[8] J.Goodman, J. Polym. Sci., 44, 551 (1960).

[9] G. J. Arguette, U. S. Patent 3,061,458 (1962).

[10] J. H. Coleman, U. S. Patent 3,068, 510 (1962).

[11] M. Stuart, Nature (London) 199, 59 (1963).

[12] A. Bradley and J. P. Hammes, J. Electrochem. Soc. 110, 15 (1963).

[13] H. Yasuda, Contemp. Top. Polym. Sci., 3, 103 (1979).

[14] H. Yasuda, Plasma Polymerization, Academic Press, Waltham (1985).

[15] H. Yasuda, Maromol. Rev., 16, 199 (1981).

[16] A. Chapiro, Radiation Chemistry of Polymers, Wiley, New York (1964).

[17] A. R. Westwood, J. Eur. Polym., 7, 363 (1971).

[18] A. Schütze, J. Y. Jeong, S. E. Babayan, J. Park, G. S. Selwyn, R. F. Hicks, IEEE Transaction on Plasma Science, 26, 6 (1998).

[19] J. Friedrich, Plasma Process. Polym. 8, 783 (2011).

[20] J. Castro, M. H. Guerra-Mutis, H. J. Dulce, Plasma Chem. Plasma Process, 23, 297 (2003).

[21] J. R. Roth, ''Industrial Plasma Engineering: Applications to Non-thermal Plasma Processing'', Vol. 2, IOP Publishing, Bristol (2001).

[22] Y. P. Raizer, ''Gas Discharge Physics'', Springer, Heidelberg (1991).

[23] E. E. Kunhardt, IEEE Trans. Plasma Sci., 28, 189 (2000).

[24] A. Schutze, J. Y. Jeong, S. E. Babayan, J. Park, G. S. Selwyn, R. F. Hicks, IEEE Trans. Plasma Sci., 26, 1685 (1998).

[25] K. H. Becker, K. H. Schoenbach, J. G. Eden, J. Phys., D39, R55 (2006).

[26] M. Laroussi, T. Akan, Plasma Process. Polym., 4, 777 (2007).

[27] H. Aizawa, T. Makisako, S. M. Reddy, K, Terashima, S. Kurosawa, M, Yoshimoto, J. Photopolym. Sci. Technol., 20 (2), 215 (2007).

[28] S. Kurosawa, H. Harigae, H. Aizawa, J. W. Park, H. Suzuki, K. Terashima, J. Photopolym.Sci. Technol., 18/2, 273 (2005).

[29] S. Kurosawa, H. Harigae, H. Aizawa, H. Suzuki, K. Terashima, J. Photopolym. Sci. Technol. 19 (2), 253 (2006).

[30] F. Massines, R. Messaoudi, C. Mayoux, Plasma Polym. 31 (1998).

[31] A. A. Radzig, B, M, Smirnov, Reference Data on Atom, Molecules and Ions (1985).

[32] N. Gomathi, A. Sureshkumar, N. Sudarsan, Curr. Sci., 94/11 (2008).

[33] D. Merche, N. Vandencasteele, F, Reniers, Thin Solid Films, 520, 4219-4236 (2012).

[34] T. P. Kasih, S. Kuroda, H. Kubota, Plasma Processes and Polymers. 4(6), 648-653, (2007).

[35] H. Yasuda, T. Hirotsu, J. Appl. Polym. Sci., 21, 3139 (1977).

[36] H. Yasuda, T. Hirotsu, J. Appl. Polym. Sci., 21, 3167 (1977).

[37] H. Kobayashi, A. T. Bell, M. Shen, J. Macromol. Sci. Chem., A10(3), 491-500 (1976).

[38] H. E. Wagner, R. Brandenburg, K. V. Kozlov, A. Sonnenfeld, P. Michel, J. F. Behnke, Vacuum, 71, 417 (2003).

[39] P. Jamroz, W. Zyrnicki, Vacuum 84, 940 (2010).

[40] J. K. Rhee, D. B. Kim, Thin Solid Films, 515, 4909 (2007).

[41] Y. Kubota, R. Ichiki, T. Hara, J. Plasma Fusion Res., Series 8, 740 (2009).

[42] C. Hudon, R. Bartnikas, M. R. Wertheimer, IEEE Trans. Electr. Insul., 28, 1 (1993).

[43] R. Brandenburg, K.V. Kozlov, N. Gherardi, P. Michel, C. Khampan, H-E. Wagner, F. Massines, Proceedings of the Eighth International Symposium on High Pressure, Low Temperature Plasma Chemistry, HAKONE VIII, Puhajarve (Estonia), 28 (2002).

[43] D. Trunec, R. Brandenburg, P. Michel, D. Pasedag, H-E. Wagner, Z. Navratil, Proceedings of the International Symposium on High Pressure, Low Temperature Plasma Chemistry, HAKONE VIII, Puhajarve (Estonia), 63 (2002).

[44] V. Poenariu, M. R. Wertheimer, R. Bartnikas, Plasma Process. Polym., 3, 17 (2006).

[45] M. Gu, J.E. Kilduff, G. Belfort, Biomaterials, 33, 1261, (2012).

[46] Y. P. Raizer, ''Gas Discharge Physics'', Springer, Heidelberg (1991).

[47] E. E. Kunhardt, IEEE Trans. Plasma Sci. 28, 189 (2000).

[48] A. Schutze, J. Y. Jeong, S. E. Babayan, J. Park, G. S. Selwyn, R. F. Hicks, IEEE Trans. Plasma Sci., 26, 1685, (1998).

[49] K. H. Becker, K. H. Schoenbach, J. G. Eden, J. Phys., D39, R55 (2006).

[50] M. Laroussi, T. Akan, Plasma Process. Polym., 4, 777 (2007).

[51] J. Laimer, H. Stŏri   Plasma Process. Polym., 4, 266 (2007).

[52] J. Laimer, H. Stŏri   Plasma Process. Polym., 3, 573 (2006).

[53] J. J. Shi, M. G. Kong, IEEE. Trans. Plasma Sci., 33, 624 (2005).

[54] J. Park, I. Henins, H. W. Herrmann, G. S. Selwyn, J. Appl. Phys., 89, 20 (2001).

[55] J. Laimer, S. Haslinger, W. Meissl, J. Hell, H. Stori, Vacuum, 79, 209 (2005).

[56] J. J. Shi, M. G. Kong, Phys. Rev. Lett., 96, 105009 (2006).

[57] S. Wang, V. Schultz von der Gathen, H. F. Dobele, Appl. Phys. Lett., 83, 3272 (2003).

[58] G. S. Selwyn, H. W. Herrmann, J. Park, I. Henins, Contrib. Plasma Phys., 6, 610 (2001).

[59] J. Park, I. Henins, H. W. Herrmann, G. S. Selwyn, J. Y. Jeong, R. F. Hicks, D. Shim, C. S.

Chang, Appl. Phys. Lett., 76, 288 (2000).

[60] J. Park, I. Henins, H. W. Herrmann, G. S. Selwyn, J. Appl. Phys., 89, 15 (2001).

[61] M. Moravej, X. Yang, G. R. Nowling, J. P. Chang, R. F. Hicks, J. Appl. Phys., 96, 7011
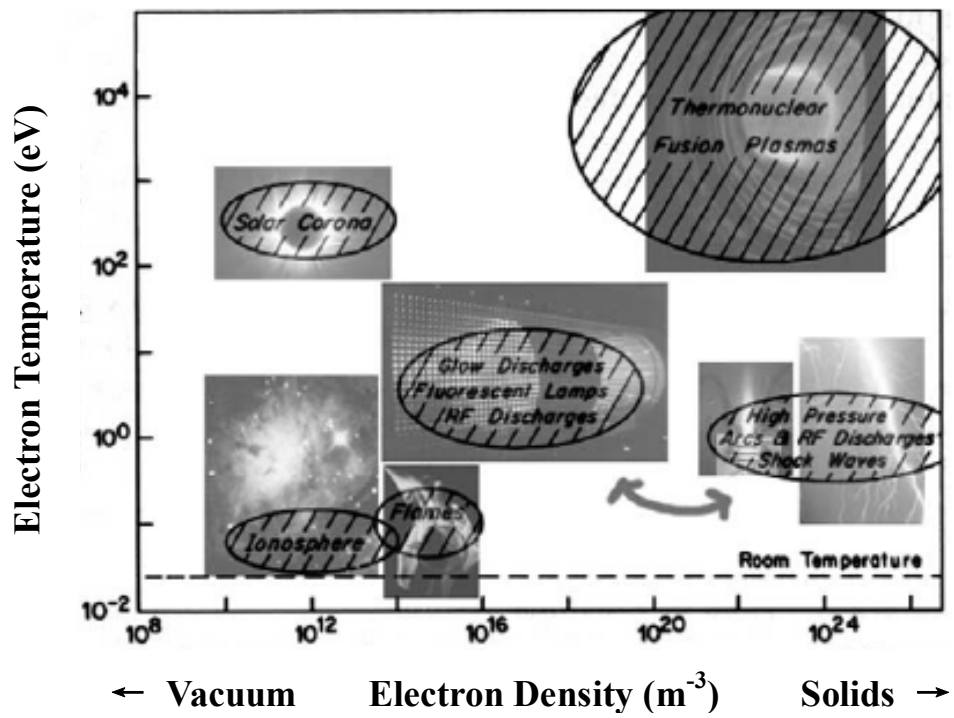
(2004).

Fig. 1-1 Schematic of plasma classification (electron temperature versus electron density).

Taken from reference [2].
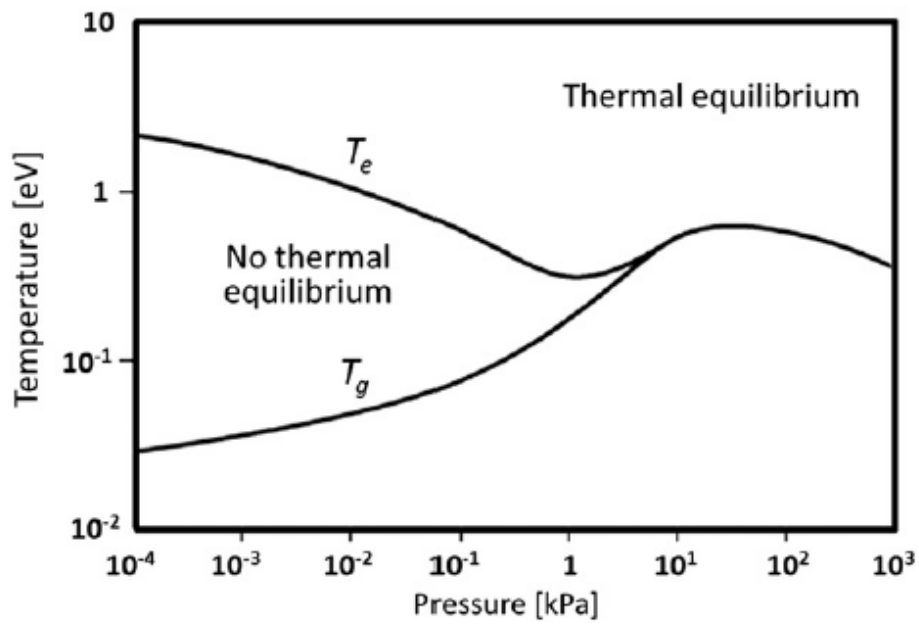
Fig. 1-2 Evolution of the temperature of the electron (T_e) and the heavy particles (T_g) as a function of the total pressure in the plasma [3].
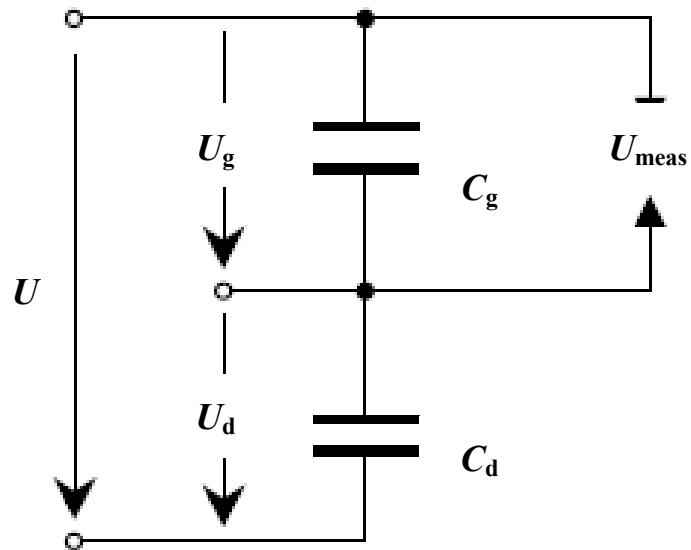
Fig. 1-3 Equivalent circuit used for DBD. Taken from reference [9].

Fig. 1-4 Experimental setup for discharge voltage, discharge current and charge transfer measurements alternatively. Using R_d for current measurement (broken line); using C_d for charge transfer measurement (solid line). Taken from reference [9].

Fig. 1-5 Idealized Q-U diagram (Lissajous figure) for measurement of dissipated electric energy per voltage cycle. Taken from reference [9].

Chapter 2 Polymerization of Styrene Induced by Atmospheric Pressure Non-Equilibrium Plasma Jet
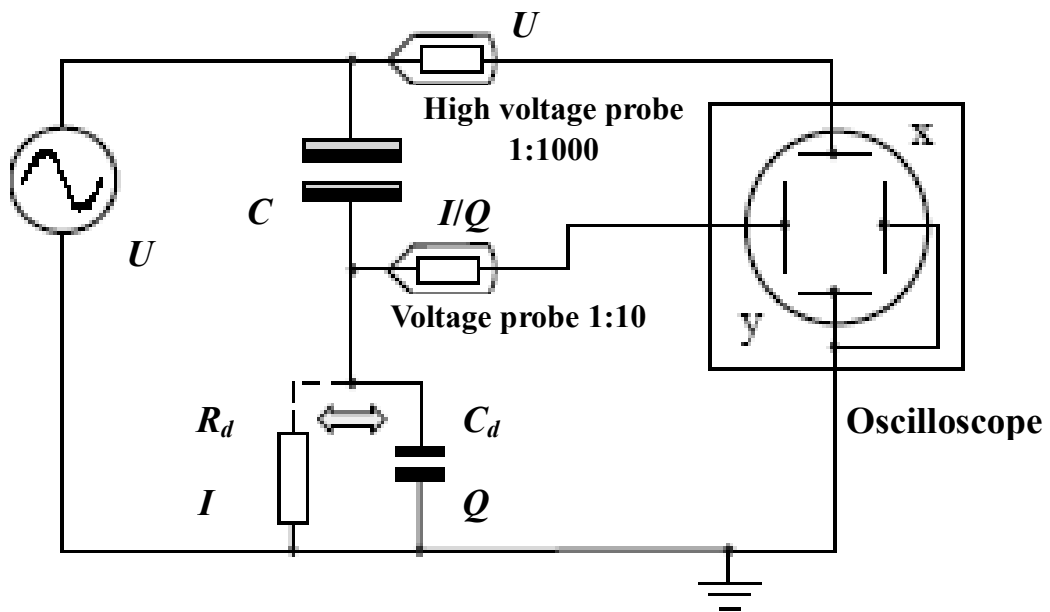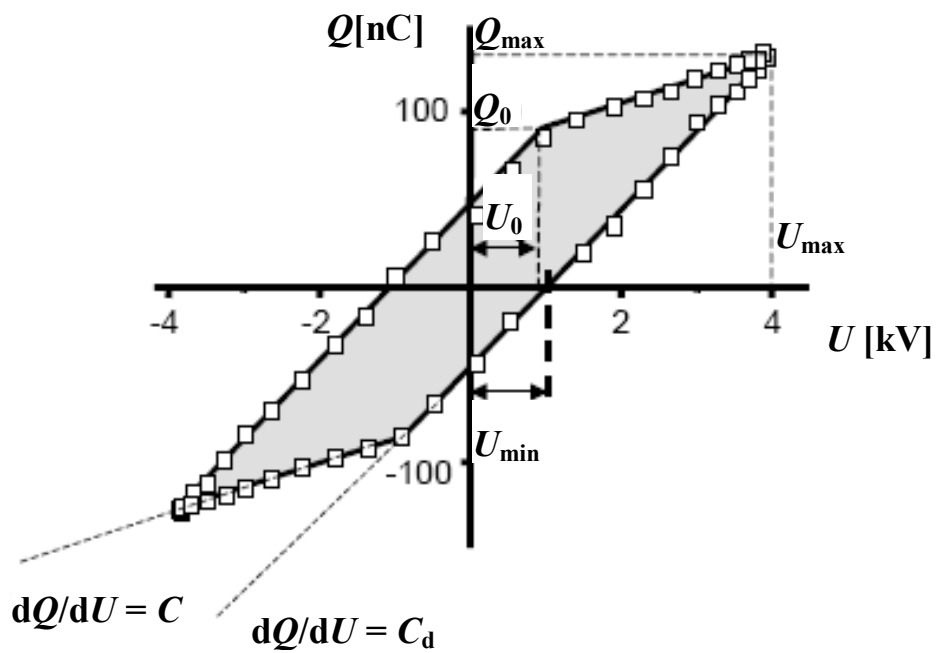
2.1 Introduction

Non-equilibrium plasmas have been used in various fields such as materials processing and biomedicine and in processes such as surface coating and plasma enhanced chemical vapor deposition (PECVD) [1-5]. Previously, non-equilibrium plasmas were typically employed at pressures between 0.1 and 500 Pa. In order to maintain the low pressure that was required for the discharge, sophisticated vacuum equipment was necessary. And, it was highly desirable to eliminate the need for expensive vacuum systems and operate plasmas at atmospheric pressure for reducing the costs. Recently, as the developing as the low gas temperature at atmospheric pressure discharge sources which include atmospheric pressure plasma jet, cold plasma torch, one atmosphere uniform glow discharge plasma and microplasma, the technology of atmospheric plasma chemical vapor deposition became easily to realize [6-13].

Generally, polymers are widely used as biomaterials due to their durability and low production cost. Among other polymers PS has commonly been applied as a disposable culture dishes because it's transparent in the visible range, and non-toxic materials [14-18].

Oran et al. [19] studied the structure of pulsed plasma deposited styrene films by time of flight static secondary ion mass spectrometry before and after exposure to ambient air. The study is dedicated to find correlations between the chemical characters of the plasma deposited styrene films and a variation of plasma deposition parameters, e.g. pulsed or cw plasma condition, duty cycle in pulsed plasma, plasma power, and monomer pressure in the reactor. Chemical properties of interest are the unsaturated, branched and/or cross-linked character of the films as well as

oxygen uptake due to aging.

In order to minimize these irregularities and to avoid the fragmentations, Friedrich et al. [20] applied low wattage and the pulsed plasma technique to investigate the retention of chemical structure and functional groups during plasma polymerization.

In the present work, the polymerization of MMA was carried out by means of the atmospheric pressure non-equilibrium helium (He) plasma jet, which is also called "CAPPLAT". The polymerization using Ar plasma under the same condition was also performed for comparison following Kasih's investigation. The results were measured by Fourier transform infrared (FT-IR) spectrum. I also used the plasma jet generator (CAPPLAT) for the polymerization of the styrene monomer and the deposited film will be analyzed by Fourier Transform Infrared spectroscopy. The electrical and optical characteristic of the plasma jet generator were also discussed. Through the results of Fourier transform infrared (FT-IR), I attempted to discuss the polymerized styrene film whether or not maintaining the primary structure induced by the Ar atmospheric pressure plasma.

2.2   Experimental setup and methods

2.2.1   Experimental monomer as the precursor

In order to clarify the polymerization conditions and discuss the mechanism of the polymerization, methyl methacrylate (MMA) and styrene were chosen for polymerization experiment. The MMA and styrene monomer were treated through reduced pressure distillation. The properties of monomers were shown in Table 2-1 [21].

2.2.2   Atmospheric pressure non-equilibrium plasma device

The originally-developed atmospheric pressure low-temperature plasma reactor used is

shown in Fig. 2-1. The plasma device used in the experiment is a hand-made cold atmospheric pressure plasma torch. The plasma torch comprises two co-axial cylindrical electrodes. With the normal connection mode, the inner electrode (an aluminum pipe, inner diameter = 7 mm and outer diameter = 8 mm) is connected to a high voltage power supply with a frequency of 20 kHz and duty of 50% (Haiden Lab SBP-10K-HF). If without specific illustration, the normal connection mode was employed in the experiments. The outer electrode (aluminum foil, width = 2 mm) is grounded. A Laboran® silicone tube (thickness: 2 mm) acts as a dielectric barrier between the two electrodes. The schematic illustration of the torch is shown in Fig. 2-2. Further details of the configuration of this plasma torch are provided in our previous papers[22-23].

Polymerization experiments of styrene were performed under normal conditions by applying invariable voltage ($\pm$ 3.0 kV~$\pm$ 4.3 kV). Ar gas was employed as the working gas and the flow rate of the Ar gas was set to 3 LPM (standard liters per minute). Styrene monomer was introduced as the additive gas into the Ar stream. Avoiding the effect of the other element, I also introduced Ar gas into the styrene monomer by the flow rates of 0.2 ~ 0.5 LPM. All flow rates were controlled using a mass flow controller. The plasma polymerization was performed in a chamber (quartz glass container). Prior to the plasma polymerization, the air in the chamber was replaced by Ar for 5 min with 3 L/min. The deposition was carried out on the KBr disk (13 mm Φ). The deposition distance was 5 mm and the deposition time was 10 min. And in order to avoid the influence of the temperature in the ambient air, the heater band was used to keep the temperature stable (30 ℃). The disk was not taken out after polymerization promptly after Ar gas was imported into the container for one minute. It should be noted that monomer was not injected directly into the Ar gas. No plasma jet was generated by such direct injection, because of the considerable quenching effect

of monomers. Therefore, I added monomers to the afterglow zone of the plasma jet through a glass capillary placed at the center of the torch (see Fig. 2-2). In this case, monomers mix with the Ar plasma in the afterglow zone.

2.2.3 Electrical measurement of Ar plasma jet

The high-voltage pulsed power with the frequency of 20 kHz, applied to achieve the plasma discharge which was measured using a 1000:1 high-voltage probe (Tektronix P6015A). The voltage probe was attached to the inner electrode of the plasma torch. The current was monitored using a wide band current monitor (Pearson TM current monitor) manufactured by Pearson Electronics Inc., Palo Alto, California, USA. The cable was passed through the wide band current monitor to monitor current. The waveforms for the total current and capacitive current were captured, so that the discharge current could be calculated. A digital phosphor oscilloscope (Tektronix TDS3012C) was inserted into the circuit to record the waveforms of voltage and current. The setup for electrical measurement is shown in Fig. 2-3.

2.2.4 Optical emission spectroscopy (OES) measurement

In addition, the optical emission spectrum (OES) measurements were performed perpendicularly to the jet by using a multi-band plasma process monitor (MPM, Hamamatsu Photonics C7460) for elucidating the polymerization mechanism.

The optical emission spectra of the plasma jet were collected perpendicular to the jet using an spectrometer (spectral range of 350–950 nm) with a resolution of 0.2 nm full width at half-maximum (FWHM); this was achieved using a personal computer equipped with relevant software (Spectra Suite) for both driving and acquisition. During the measurement of the optical emission spectra, the exposure time was 100 ms. Emission intensities of the active species were

collected at an axial position of the plasma jet, through an optical fiber with a diameter of 100 μm.

2.2.5 Fourier transform infrared (FT-IR) measurement

Transmission mode for the IR spectra of the films was taken with a Fourier Transform Infrared (FT/IR-8000, Jasco, Japan) with 64 scans at 2 cm^{-1} resolution.

2.3 Results and discussion

2.3.1 Polymerization of methyl methacrylate induced by the CAPPLAT

In order to clarify the necessary conditions for the polymerization with maintaining the primary structure of monomer, helium (He) was used to be as working gas to polymerize the MMA monomer, and the polymerized film was shown in Fig. 2-4 comparing with the polymerized film induced by Ar plasma jet. As is shown in Fig. 2-4, the polymerized MMA by He plasma was recognized to have more disordered structure judging from its broadened C-O-C absorption in Fourier transform infrared (FT-IR) spectrum. The obtained results showed that Ar plasma can polymerize MMA more efficiently than He plasma not only in terms of polymerization rate but also polymer composition.

This observation brought a working hypothesis that a monomer of which ionization potential (9.70 eV for MMA) is close to or larger than the energy of metastable atom in plasma can be polymerized easily with retaining the primary structure. In order to support this working hypothesis the styrene was discussed below, which ionization potential is as small as 8.50 eV.

2.3.2 Electrical characterization of Ar plasma jet

Normally, in dielectric barrier discharge, electrodes are separated by a distance of few millimeters to ensure the stable plasma ignition [24], but our plasma torch is based on dielectric barrier discharge principal. There is no space between electrode and dielectric barrier so we need

not to consider the sheath effect also. Depending on working gas composition, voltage and frequency of excitation, the discharge can be filamentary or glow [25, 26], Dielectric barrier limits the discharge current and distributes the steamers randomly on the electrode surface in order to achieve homogeneous discharge. Fig. 2-5 shows the wave forms for nominal applied voltage (blue line) and total current (red line). The nominal applied voltage was ± 4 kV (peak to peak) but the voltage according to the waveform, shown in Fig. 2-5, is about ± 3.8 kV (peak to peak). The drop in potential is because of the ionization of the gas and subsequent charge accumulation. The waveform also shows the square waveform of the voltage with 50% duty cycle. The current form in the circuit is about 0.2 A.

Fig. 2-6 shows typical waveforms of the applied voltage (blue line) and total current (red line) recorded by the oscilloscope when the styrene monomer was introduced to the plasma jet from the capillary.

And the comparison of waveform of total current in Ar discharge before addition of styrene (blue line) and the total current after addition of styrene (red line) is shown in Fig. 2-7. It is apparent that injecting styrene monomer to the plasma afterglow zone through a glass capillary did not change the current of this Ar plasma jet. So, the plasma jet itself was regarded not to be affected by the monomer addition.

As Tepper et al. [27] demonstrated, dielectrics are capable of accumulating appreciable amounts of charges on the surface in order to diffuse glow discharge from the CAPPLAT. The charges are trapped uniformly on the surface, which was supported by the applied voltage. When the electric field changes its polarity and exceeds a certain threshold value, the charge carriers are expelled spontaneously from the surface and initiate a homogeneous discharge. Obviously, when

the styrene monomer is traduced into the plasma jet, less electron density, less pre-ionization and subsequently less avalanches for diffuse glow discharge is obtained, which cause a decrease in the total current.

Therefore, a simple discharge mechanism is proposed here. First, Ar molecules are excited and ionized through collisions with energetic electrons. In this step, energy is transferred to the Ar particles and the Ar active species (Ar metastable atoms) are produced. Second, styrene monomer is excited through collisions with energetic Ar metastable atoms. This suggests that the plasma jet was quenched by the styrene monomer, which was added to the plasma afterglow zone through the glass capillary.

2.3.3 Optical characterization of Ar plasma jet

2.3.3.1 Typical optical emission spectrum

A typical optical emission spectrum of CAPPLAT Ar plasma jet in the wavelength range of 350–950 nm is shown in Fig. 2-8. It can be seen that peaks belonging to the excited Ar atoms (4p-4s transition) are predominant in this plasma jet (in the wavelength range of 690–950 nm) [28-31], which the reaction process (1) ~ (3) was represented.

$$e^* + Ar^0 \rightarrow Ar^m + e \tag{1}$$

$$e^* + Ar^m \rightarrow Ar^*(4p) + e \tag{2}$$

$$Ar^*(4p) \rightarrow Ar^*(4s) + h\nu \tag{3}$$

Ar plasma generates many species: ions (Ar^0, Ar^+, and Ar^{2+}), Ar^m, electrons (e), neutrals and so on. Mostly, Ar^m contains $^3P_0$ for 11.72 eV and $^3P_2$ for 11.55 eV. Ar^m ($^3P_2$) of which excitation energy is 11.55 eV plays an important role since the lifetime of $^3P_2$ is 38s and longer than that of $^3P_0$, 1.3s [32, 33]. Therefore, Ar^m ($^3P_2$) plays an important role in the Ar plasma.

Some peaks at 357 nm belonging to the N_2 second positive system and an OH at 308 nm were also observed with relatively Ar atom strong emission intensities [34-36]. It is thought that N_2 and OH active species were detected in the pure Ar discharge maybe the impurities from the Ar gas were excited and dissociated. However, as above mentioned, the ionization of N_2 and OH through collisions with energetic electrons is negligible in CAPPLAT Ar plasma jet, since the electron density and the electron energy are relatively low. In Ar discharge, Ar metastable atoms play the leading role in the polymerization reaction because they are generated by collisions with energetic electrons. Emission intensities and assignments of Ar active species (in the wavelength range of 350–950 nm) detected in CAPPLAT Ar plasma jet are summarized in Table 2-2.

2.3.3.2 Effect of additive gas (styrene) on polymerized OES

As is shown in Fig. 2-9 is that the OES of the plasma jet with and without styrene monomer. From the Fig. 2-9, when the styrene monomer was introduced to the plasma jet, there is no any other active species occurred and the emission lines from the excited species do not seem to be changed. But the emission intensity became weaker when the monomer was imported. This can be interpreted that the styrene monomer is the quencher to the Ar gas.

2.3.3.3 Effect of voltage on polymerized OES

The OES of the plasma jet with styrene monomer by changing the voltage is shown in Fig. 2-10. From the Fig. 2-10, the distribution of emission lines from the excited species do not seem to be changed even when the voltage was increased. But, it became stronger by increasing the voltage. The increased density means the hv increased in the reaction 3 as mentioned above, which can deduce that the Ar^* (4p) and Ar^m densities were also increased in the reaction 2 and reaction 1 separately. In other words, the density of Ar^m could be changed by adjusting the voltage, which is

the different to the vacuum plasma.

Therefore, it is concluded that when the voltage is increased, the Ar metastable density is also increased, which agrees with the conclusion [37, 38]. And the Ar metastable density is becoming larger resulting from the voltage is increased will be bring an increase in the rate of reaction.

2.3.3.4 Effect of additive gas flow rate on polymerized OES

The OES of the plasma jet with styrene monomer by changing the carrier gas flow rate is shown in Fig. 2-11. From the Fig. 2-11, the distribution of emission lines from the excited species do not seem to be changed even when the carrier gas flow rate was changed. When the carrier gas increased, the OES intensity became weaker. It is thought the quenching effect became obviously.

2.3.4 Chemical Structure of the Plasma Deposited Films by FT-IR

The comparison of FT-IR spectrum between standard polystyrene and plasma polymerized styrene monomer was shown in Fig. 2-12.

In the surface of the sample, there are some tiny particles. As is shown in Fig. 2-12, it is obviously observed that the C=H bond peak at 702 cm^{-1}, 760 cm^{-1} assigned to out-of-plane deformation bending. And the intensity of appeared peaks at the 1450 cm^{-1} ~ 1600 cm^{-1} became weaker ,which were induced by C=C bond of benzene ring and the frame vibration in the aspect of the derivate. The nearby 3000 cm^{-1} ~ 3080 cm^{-1} peaks were induced by stretching vibration among C-H group of aromatic ring. And the intensity of those peaks almost disappeared. The peaks also disappeared at 1825 $\pm$ 175 cm^{-1} which were absorption induced by C-H vibration of polystyrene aromatic ring. From mentioned above, it is said that styrene was ionized by Ar plasma basing on the Penning Ionization.It was unfortunately the deposited product was the oxidized polymeric compound, so the deposit would be a by-product of plasma processing of styrene.

2.4   Conclusions

In this study, the polymerization of MMA was carried out by means of an atmospheric pressure non-equilibrium helium (He) plasma jet. The polymerization using Ar plasma under the same condition was also performed for comparison following Kasih's investigation. The obtained results showed that Ar plasma can polymerize MMA more efficiently than He plasma not only in terms of polymerization rate but also polymer composition. This observation brought a working hypothesis that a monomer of which ionization potential is close to or larger than the energy of metastable atom in plasma can be polymerized easily with retaining the primary structure. This working hypothesis was supported by the fact that styrene of which ionization potential is as small as 8.50 eV, much lower than Ar^m energy, was hardly polymerized by Ar plasma.

In order to discuss styrene monomer polymerization with atmospheric pressure Ar plasma jet, OES technique and FT-IR were used to analyze emission density of plasma jet and the structure of polymerized films respectively. OES study showed there is no other atom appeared in plasma phase when the admixed styrene was flowed by a flux of Ar carrier gas. The results were wn in Fig. 2-10 and Fig. 2-11 indicates that the deposition rate increased as the applied voltage and the monomer feed ratio increasing. However, from the FT-IR analyses, it is confirmed that plasma-polymerized styrene films were not polymerized by the Ar plasma in spite of keeping some functional groups of styrene molecule. The FT-IR results were consistent with the working hypothesis, which speculated that a monomer of which ionization potential is close to or larger than the energy of metastable atom can be polymerized easily with retaining the primary structure.
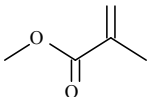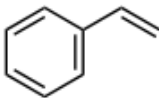
References

[1] S. Yang, H. Yin, Plasma Chem. Plasma Process, 27, 23 (2007).

[2] R. B. Gadri, J. R. Roth, T. C. Montie, K. K. Wintenberg, P. P. Y. Tsai, D. J. Helfritch, P. Feldman, D. M. Sherman, F. Karakaya, Z. Chen, Surf. Coat. Technol., 131, 528 (2000).

[3] S. Martin, F. Massines, N. Gherardi, C. Jimenez, Surf. Coat. Technol., 177-178, 693 (2004).

[4] M. Walker, K. M. Baumgărtner, J. Feichtinger, M. Kaiser, A. Schulz, E. Răuchle, Vacuum, 57, 387 (2000).

[5] M. F. Dubreuil, E. M. Bongaers, Surf. Coat. Technol., 202, 5036 (2008).

[6] J. Park, I. Henins, H. W. Herrmann, G. S. Selwyn, J. Appl. Phys., 89, 20 (2001).

[7] M. Laroussi, T. Akan, Plasma Process. Polym., 4, 777 (2007).

[8] Y. H. Kim, Y. H. Choi, J. K. Park, W. T. Ju, K. H. Paek, Y. S. Hwang, Surf. Coat. Technol., 174-175, 535 (2006).

[9] L. Xu, P. Liu, R. J. Zhan, X. H. Wen, L. L. Ding, M. Nagatsu, Thin Solid Films, 506, 400 (2006).

[10] J. Zhang, J. Sun, D. Wang, X. Wang, Thin Solid Films, 506, 404 (2006).

[11] Y. Tanaka, S. Iizuka, Thin Solid Films, 506, 436 (2006).

[12] C. Cheng, L. Zhang, R. J. Zhan, Surf. Coat. Technol., 200, 6659 (2006).

[13] F. Massines, P. Ségur, N. Gherardi, C. Khamphan, A. Ricard, Surf. Coat. Technol., 174-175, 8 (2003).

[14] N. Inagaki, Plasma polymerization. Technomic Publishing Co, Inc., Pennsylvania (1996).

[15] B. Mitu, S. Bauer-Gogonea, H. Leonhartsberger, M. Lindner, S. Bauer, G. Dinescu, Surf. Coat. Technol., 174-175, 124 (2003).

[16] D.S. Kumar, Y. Yoshida, Surf. Coat. Technol., 169-170, 600 (2003).

[17] I. S. Bae, S. H. Cho, Y. S. Park, B. Hong, Z. T. Park, J. G. Kim, J. H. Boo, Thin Solid Films, 506-507, 2 (2006).

[18] H. K. Yasuda, Plasm Process. Polym., 2, 293-304 (2005).

[19] U. Oran, S. Swaraj, J. F. Friedrich, W. E. S. Unger, Surf. Coat. Technol., 200, 463 (2005).

[20] J. F. Friedrich, I. Retzko, G. Kühn, W.E.S. Unger, A. Lippitz, Surf. Coat. Technol., 142-144, 460-467 (2001).

[21] http://www.chemindustry.com/apps/chemicals

[22] X. Fei, Y. Kondo, X. Qian, S. Kuroda, T. Mori, K. Hosoi, Key Engineering Materials, 596, 65-69 (2014).

[23] J. Yan, Y. Kondo, X. Qian, X. Fei, K. Hosoi, T. Mori, S. Kuroda, Applied Mechanics and Materials, 423-426, 537-540 (2013).

[24] C. Tendro, C. Tixier, P. Tristant, Desmasion, and P. Leprince. Spectrochimica Acta Part B 61, (2005). [26] SCIGRESS Mo Compact 1.0 User Guide.

[25] F. Massines, and G. Gouda. J. Phys. D: Appl. Phys. 31, 3411, (1998).

[26] T. Yokohama, M. Kogoma, T. Moriwaka, and S. Okazaki. J. Phys. D: Appl. Phys. 23, 1125, (1990).

[27] J. Tepper, M. Lindmayer, and J. Salge. Hakone VI, Cork, Ireland. 123, (1998).

[28] Q. S. Yu, H. K. Yasuda. Plasma Chem. Plasma Process, 18, 461 (1998).

[29] M.C. García, M. Varo, P. Martínez, Plasma Chem. Plasma Process, 30, 241 (2010).

[30] K. Hiraoka, S. Fujimaki, S. Kambara, H. Furuya and S. Okazaki, Rapid Commun. Mass Spectrom, 18, 2323-2330 (2004).

[31] Y. Harada, S. Masuda, H. Ozaki, Chem. Rev. 97, 1897-1952 (1997).

[32] H. Katori and F. Shimizu, Phys. Rev. Lett. 70, 3545 (1993).

[33] R. S. Van Dyck, Jr., C. E. Johnson and H. A. Shugart, Phys. Rev. A 5, 991 (1972).

[34] A. F. Bublievskii, A. A. Galinovskii, A. V. Gorbunov, S. A. Zhdanok, V. A. Koval, L. I. Sharakhovskii, G. V. Dolgolenko, D. S. Skomorokhov, J. Eng. Phys. Thermophys, 79, 629 (2006).

[35] V. Poenariu, M. R. Wertheimer, R. Bartnikas, Plasma Process. Polym, 3, 17 (2006).

[36] J. Kuba, L. Kucera, F. Plzak, M. Dvorak, J. Mraz, Coincidence Tables for Atomic Spectroscopy, Elsevier Publishing Company (1965).

[37] Y. K. Lee, K. T. Hwang, M. H. Lee and C. W. Chung, J. Korean Phys. Soc. 52 (6), 1792 (2008).

[38] M. V. Malyshev and V. M. Donnelly, Phy. Rev. E 60, 6016 (1999).

Table 2-1 The properties of polymerized monomer list

Monomer	Molecular Formular	Chemical Formular	Molecular Weight (g/mol)	Density (g/cm^3)	Boiling Point (℃)
MMA	$C_5H_5O_2$		100.12	0.944	100
Styrene	C_8H_8		104.15	0.906	145

Table 2-2 Summary of active species (wavelength range of 350–950 nm) detected in CAPPLAT Ar plasma jet at a distance of 5 mm from the end of torch. Discharge conditions: pure Ar discharge at a flow rate of 3 LPM, dielectric thickness of 2 mm, nominal applied voltage of ± 4.0 kV (peak to peak) with 50% duty cycle, discharge frequency of 20 kHz.

| Species	λ (nm)	Absolute irradiance (μW/cm^2/nm)	Transition
N$_2$ 2nd positive system	357.51	0.01717	C$^3\prod_u \rightarrow$ B$^3\prod_g$
Ar atoms	696.53	0.0836	4p $\rightarrow$ 4s
	707.60	0.0049	
	728.03	0.0239	
	739.22	0.0124	
	751.67	0.0484	
	764.06	0.2036	
	773.03	0.1764	
	795.47	0.0295	
	801.91	0.0489	
	812.00	0.1031	
	827.13	0.1889	
	842.87	0.0709	
	852.57	0.0192	
	867.57	0.0021	
	912.68	0.2654	
	922.70	0.0351	
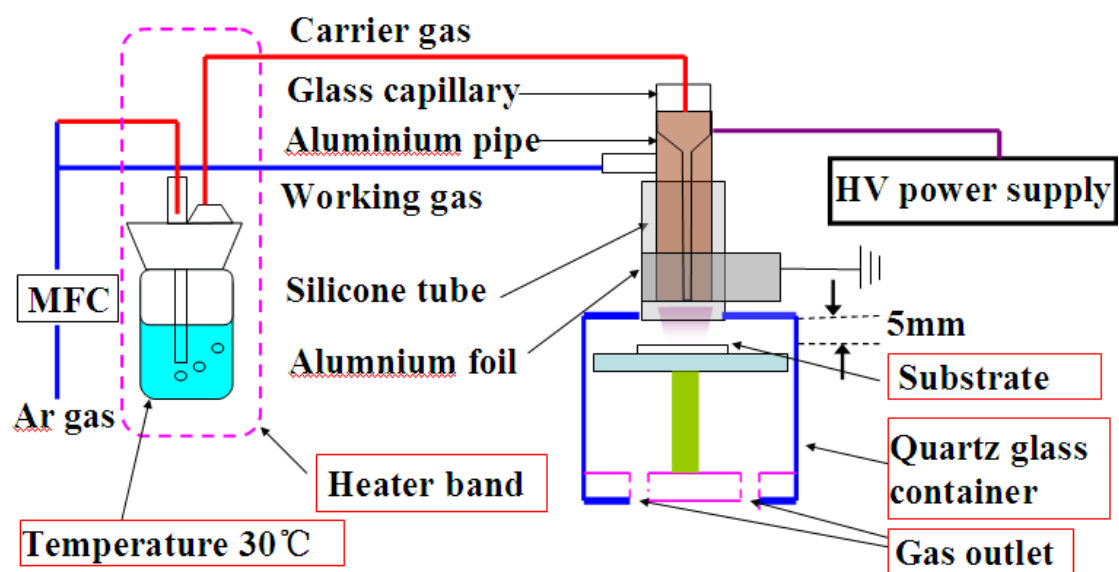
Fig. 2-1 Schematic diagram for atmospheric pressure non-equilibrium plasma polymerization.
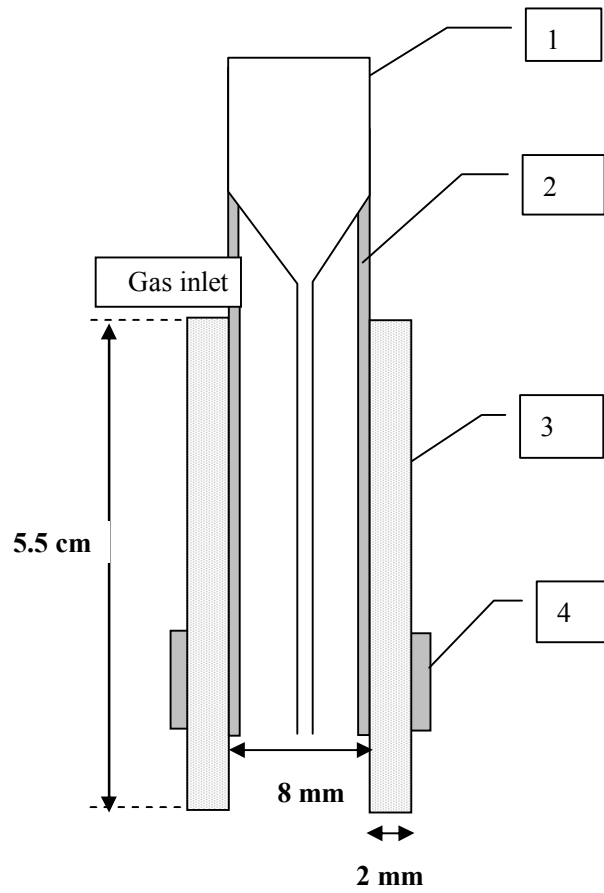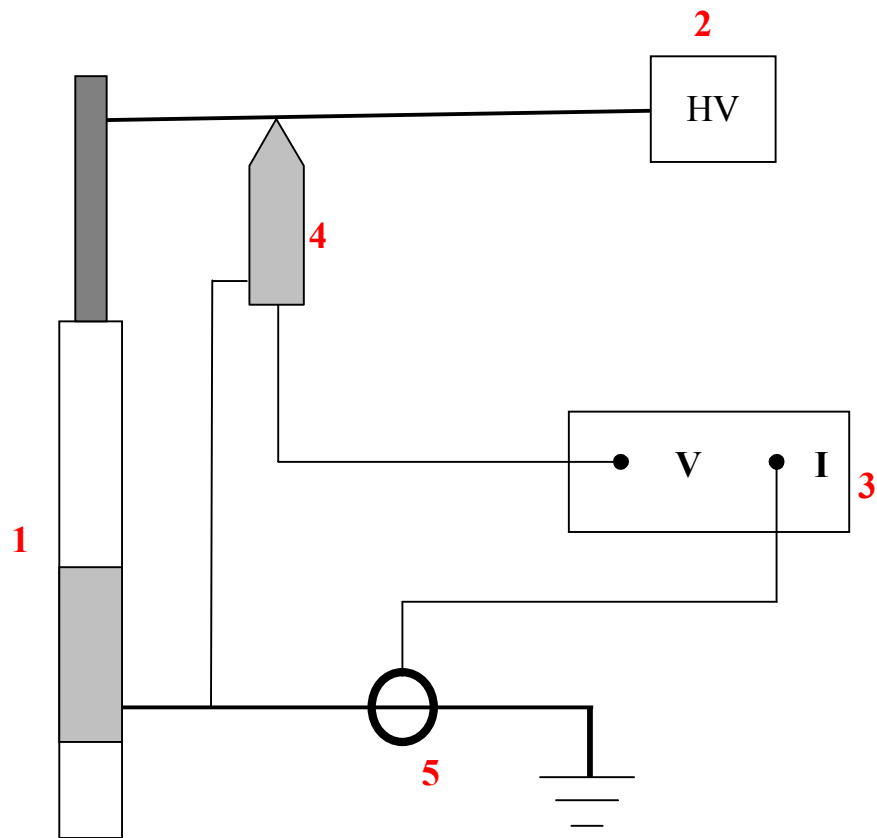
a: front view of CAPPLAT torch
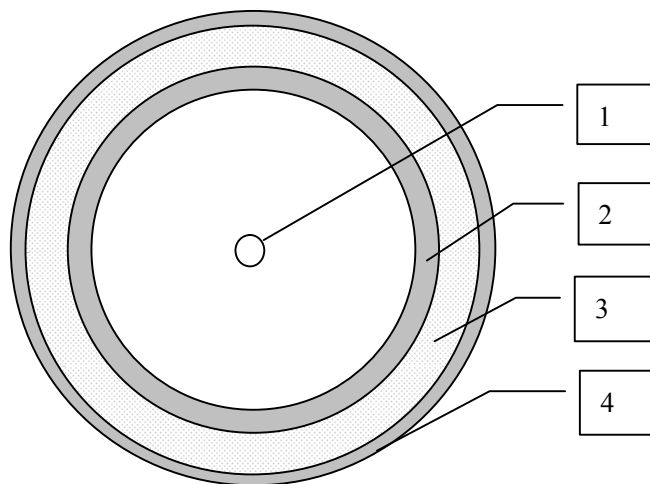
b: top view of CAPPLAT torch

Fig. 2-2 Schematic illustration of CAPPLAT plasma torch. (a): front view of CAPPLAT torch; (b): top view of CAPPLAT torch.
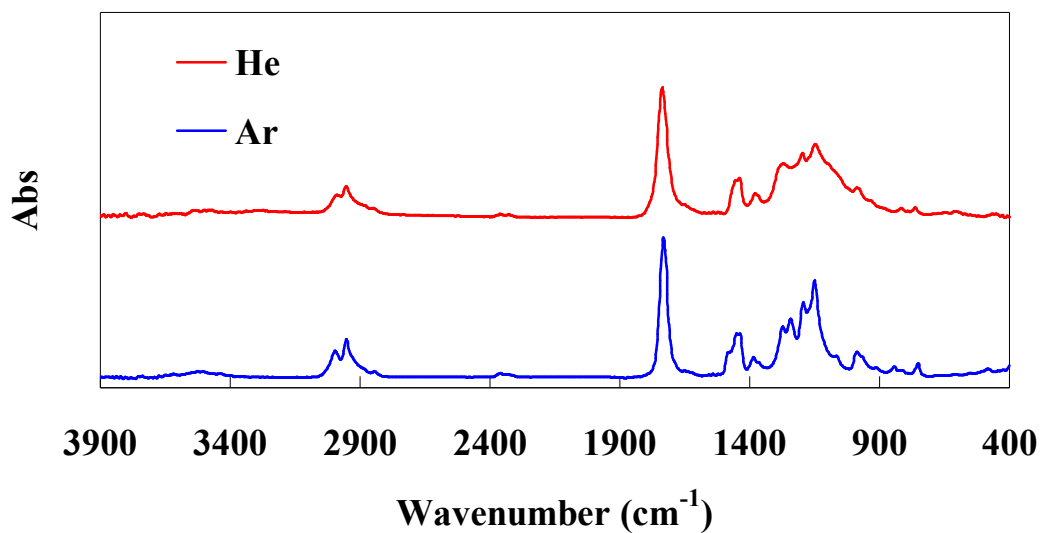
1: glass capillary; 2: inner electrode; 3: dielectric; 4: outer electrode.

Fig. 2-3 Electrical measurement setup for CAPPLAT Ar plasma jet.

1: CAPPLAT plasma torch; 2: High-voltage pulsed power source; 3: Oscilloscope; 4: High-voltage probe; 5: Current probe.

Fig. 2-4 The comparison of polymerized MMA FT-IR absorption spectrums induced by He plasma jet (red line) and Ar plasma jet (blue line). Discharge conditions: pure Ar discharge at a flow rate of 3 L/min, carrier gas 0.5 L/min, dielectric thickness of 2 mm, nominal applied voltage of ± 4.0 kV (peak to peak) with 50% duty cycle, discharge frequency of 20 kHz, deposition time of 10min.
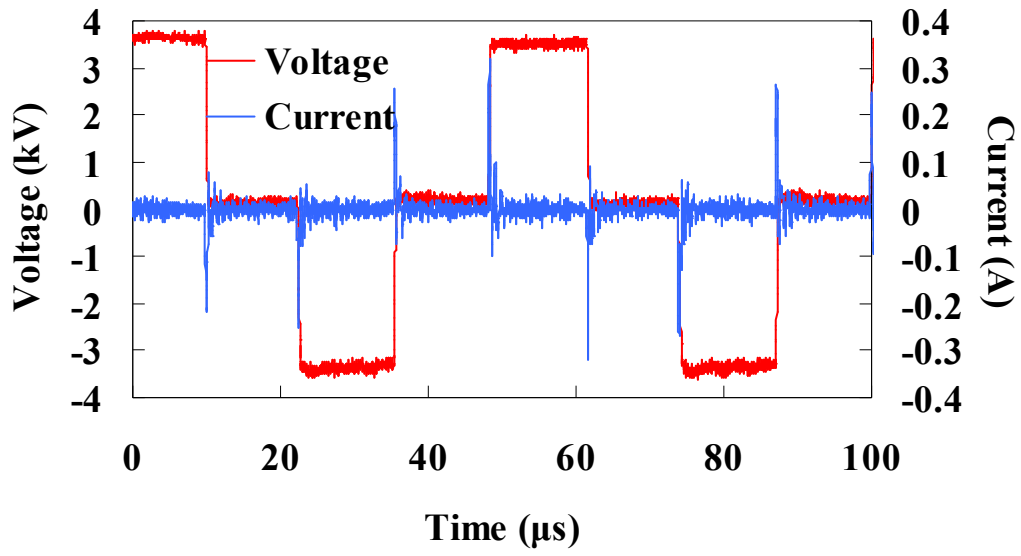
Fig. 2-5 Typical waveform of applied nominal voltage Vpp ± 4 kV (red line) voltage and the
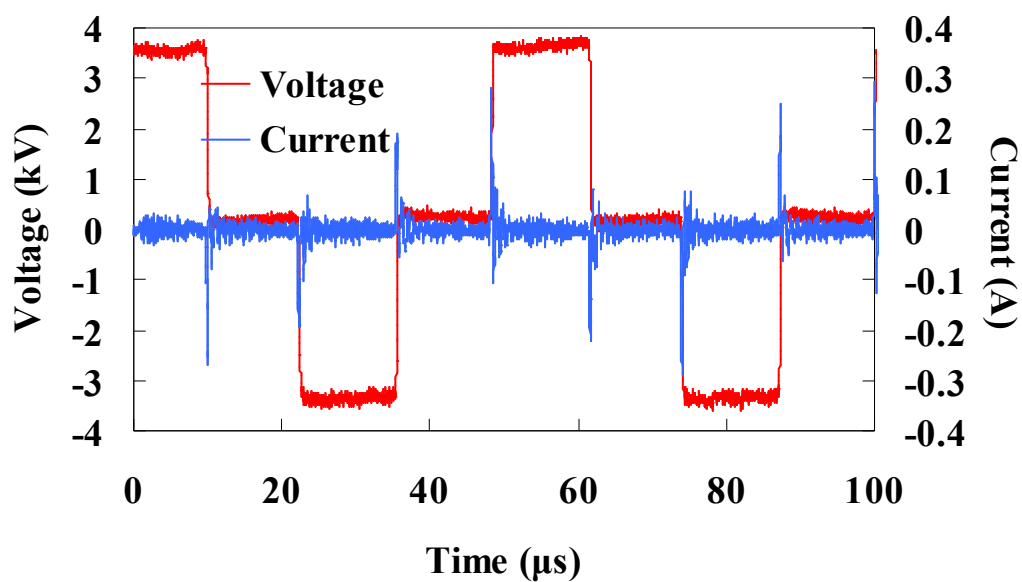
total current (blue line); Ar (3 L/min).

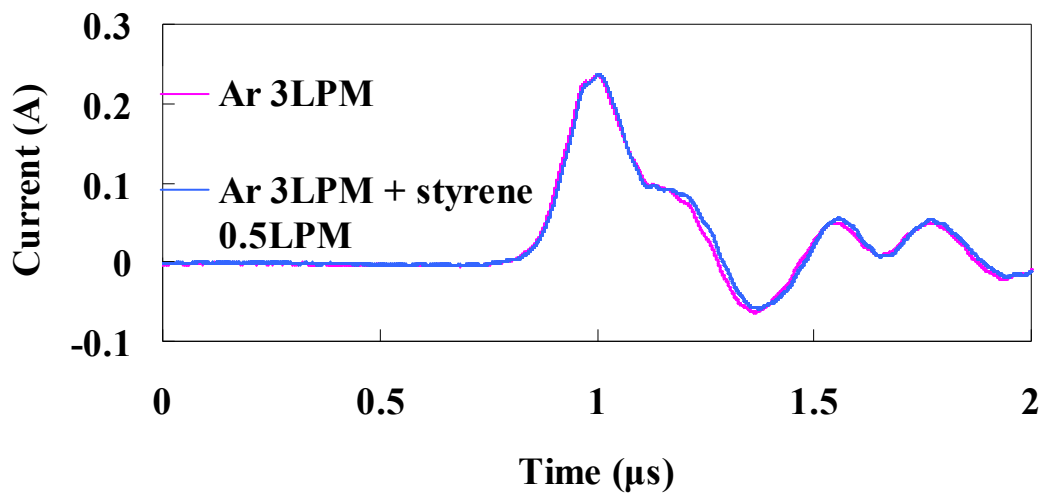**Fig. 2-6 Typical waveform of applied nominal voltage Vpp ± 4 kV (red line) voltage and the total current (blue line); Ar (3 L/min) carried the vapor of styrene (0.5 L/min) to the plasma jet through the capillary.**

Fig. 2-7 Comparison of waveform of total current in Ar discharge before addition of styrene (pink line) and the total current after addition of styrene (blue line) during plasma change.
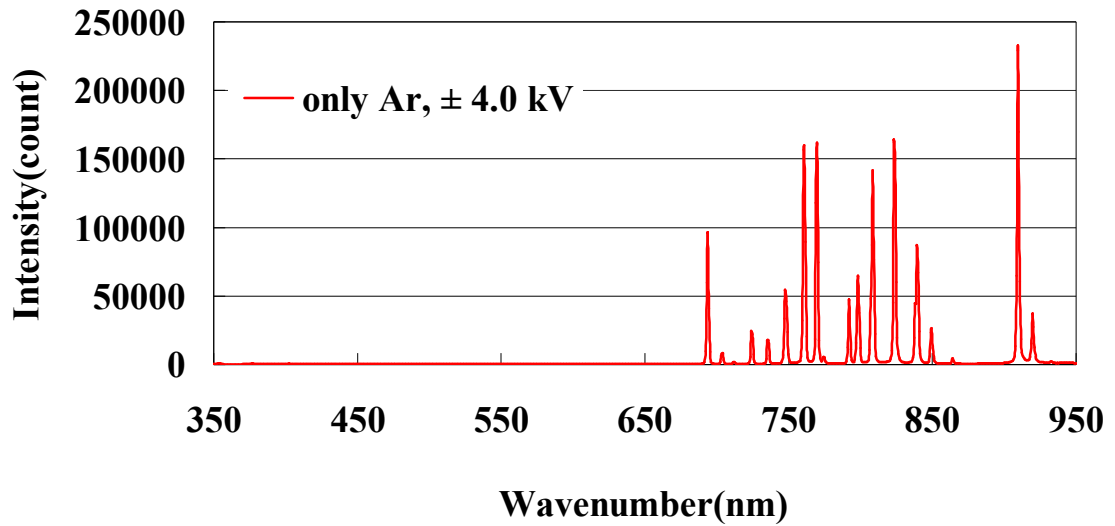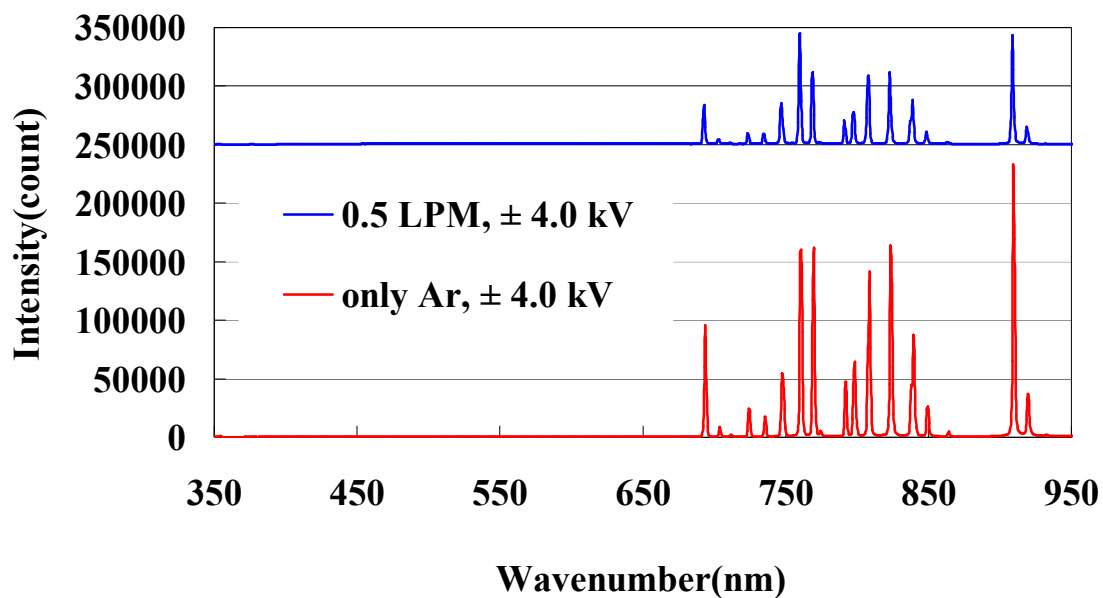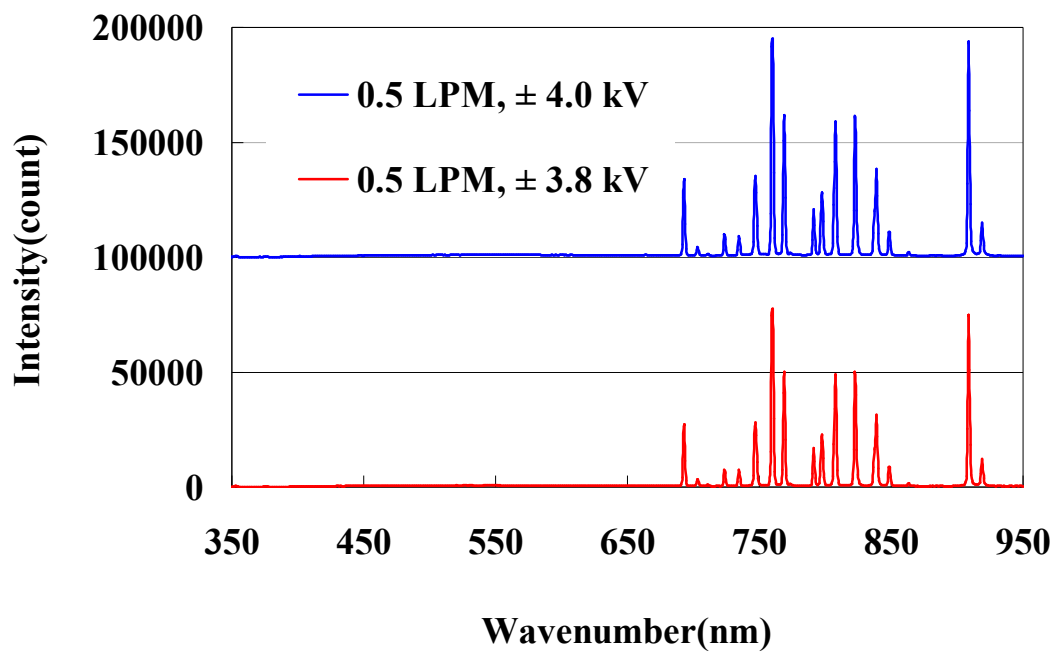
Fig. 2-8 Typical optical emission spectrum of CAPPLAT Ar plasma jet measured at a distance of 5 mm from the end of torch. Discharge conditions: pure Ar discharge at a flow rate of 3 LPM, dielectric thickness of 2 mm, nominal applied voltage of ± 4.0 kV (peak to peak) with 50% duty cycle, discharge frequency of 20 kHz.
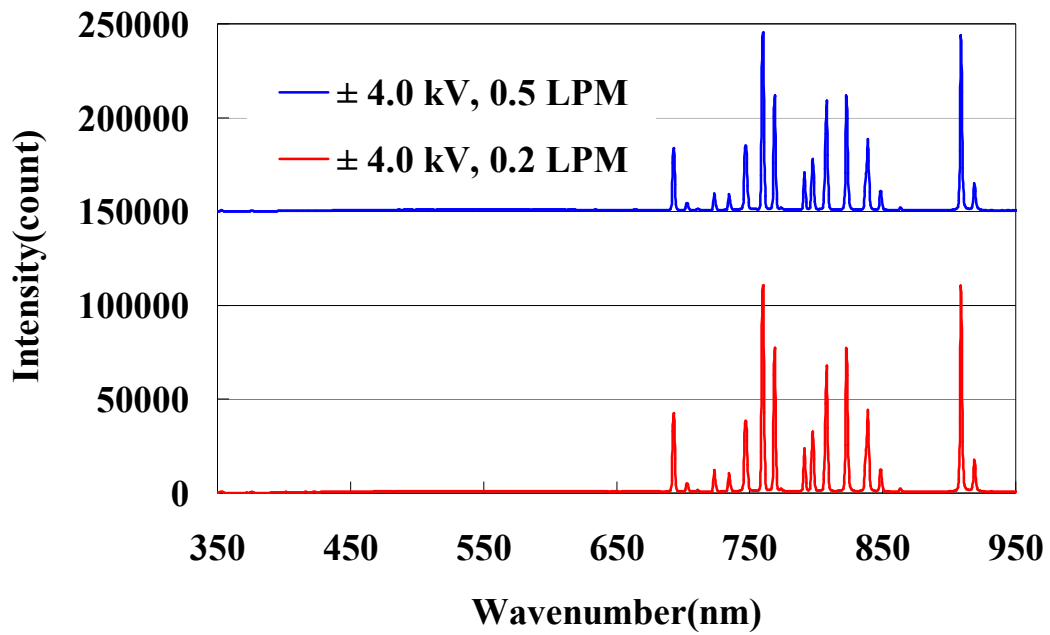
Fig. 2-9 Optical emission spectra of plasma jet with and without monomer measured at a distance of 5 mm from the end of torch. Discharge conditions: pure Ar discharge at a flow rate of 3 L/min, carrier gas flow 0.5 L/min, dielectric thickness of 2 mm, nominal applied voltage of ± 4.0 kV (peak to peak) with 50% duty cycle, discharge frequency of 20 kHz.

Fig. 2-10 Optical emission spectra of plasma jet with monomer at different voltage measured at a distance of 5 mm from the end of torch. Discharge conditions: pure Ar discharge at a flow rate of 3 L/min, carrier gas flow 0.5 L/min, dielectric thickness of 2 mm, nominal applied voltage of ± 3.8 kV and ± 4.0 kV (peak to peak) with 50% duty cycle, discharge frequency of 20 kHz.

Fig. 2-11 Optical emission spectra of plasma jet with monomer at different carrier gas flow measured at a distance of 5 mm from the end of torch. Discharge conditions: pure Ar discharge at a flow rate of 3 L/min, carrier gas flow 0.2 L/min and 0.5 L/min, dielectric thickness of 2 mm, nominal applied voltage of ± 4.0 kV (peak to peak) with 50% duty cycle, discharge frequency of 20 kHz.
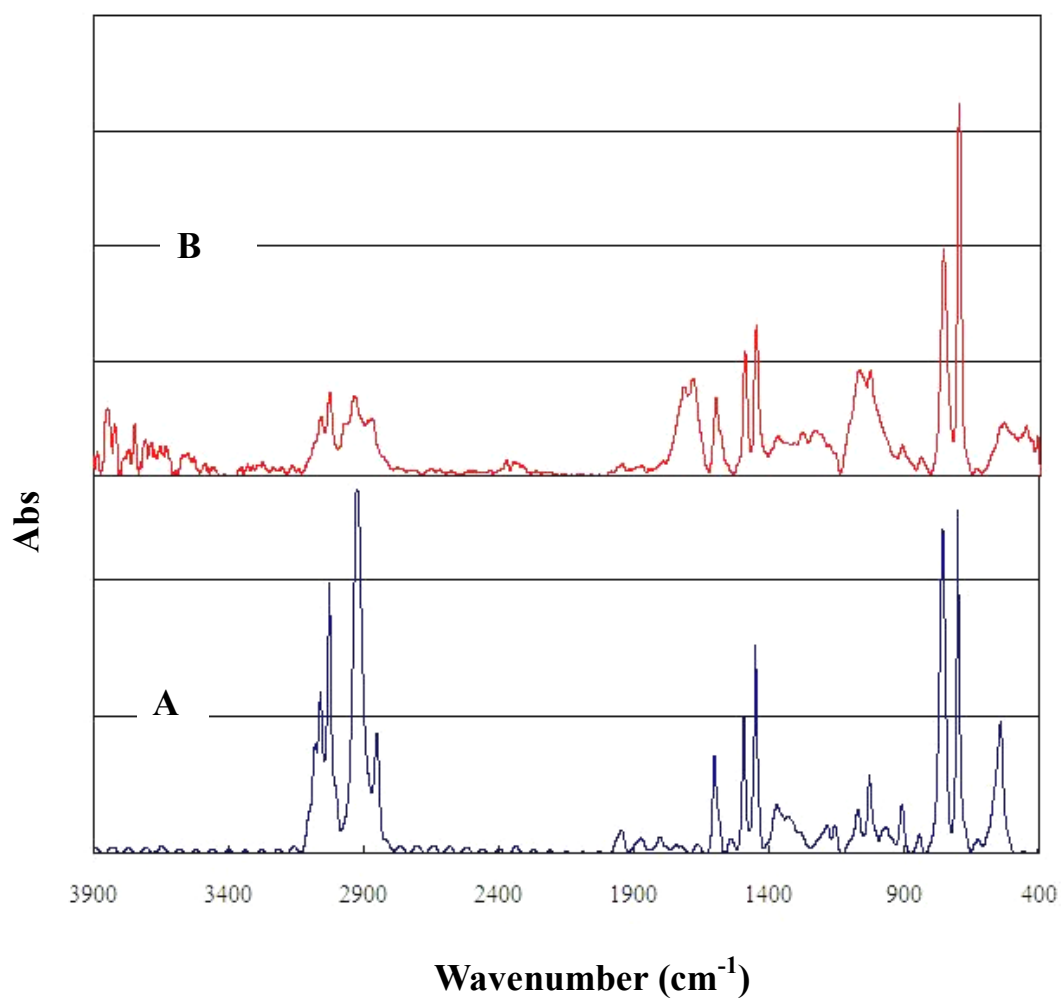
Fig. 2-12 The comparison of IR absorption spectrum between standard polystyrene (A) and plasma deposited styrene (B). Discharge conditions: pure Ar discharge at a flow rate of 3 L/min, carrier gas 0.5 L/min, dielectric thickness of 2 mm, nominal applied voltage of ± 4.0 kV (peak to peak) with 50% duty cycle, discharge frequency of 20 kHz, deposition time of 10min.

Chapter 3 Polymerization of Methacryl Acid Derivatives Induced by Atmospheric Pressure Non-Equilibrium Plasma Jet

3.1 Introduction

As for the polymerization using the low-temperature plasma, many studies have been reported [1-6]. And, utilizing the low-temperature atmospheric pressure plasma jet, which has been commercialized under the name of "CAPPLAT" by Cresur Corporation of Japan [7], both chemical vapor deposition (CVD) and polymer surface treatment have been studied previously [8-11].

Kasih et al. [9] developed the non-equilibrium atmospheric-pressure plasma torch that can be generated either in He or Ar gas by using a pulsed high voltage power supply. The hexamethyldisiloxane (HMDSO) precursor diluted in an oxygen carrier gas system was used to deposit silicon dioxide films by this torch. In terms of both quality and deposition rate at the same applied power, frequency, and gas composition, it is concluded that Ar plasma is more powerful than He plasma for depositing SiO_2-like films. When a small amount of nitrogen (N_2) added to the Ar as a working gas, the discharge behavior is transformed from filamentary to glow.

Kuwabara et al. [10-11] described the chemical vapor deposition (CVD) for thin film using the low temperature surface discharge plasma torch, and obtained an inorganic composition with a state of SiO_2 film.

And also, plasma polymerized methyl methacrylate (PPMMA) films were deposited by using argon (Ar) gas. It was found that, when raising the concentration of vaporized monomer to a certain level into the plasma, the plasma transitioned from a filamentary to a glow-like discharge, this resulting in a high retention of the monomer structure [12].

Because of the good biocompatibility, it makes methacryl acid calss monomers excellent candidate for the biomedical and pharmaceutical [13-18]. For example, poly (2-hydroxyethyl methacrylate) (poly (HEMA)) surfaces have many technological applications; these include separation devices [19-20], textile strengthening [21], adhesion [22], biocompatibility [23], and biosensors [24].

In Chapter 2, the ionization potential of styrene is as small as 8.50 eV supporting the working hypothesis, which was hardly to maintain the primary structure. So it was thought the monomer of which ionization potential is close to or larger than the energy of metastable atom is easy to keep the primary structure.

In the present work, I use the originally-developed atmospheric pressure low-temperature plasma jet generator (CAPPLAT) for the polymerization of the methacryl acids derivatives to ascertain the working hypothesis in Chapter 2. According to relationship between the rare gas excitation energy and the ionization quantum yields, by the effect of Ar metastable atom c-C_6H_{12} ionization quantum yield was almost 0.5. Meanwhile, the ionization quantum yield of CH_3OCH, $CH_3OC_2H_5$ and n-C_3H_7OH were about 0.3, C_2H_5OH even reached to the 0.1 [25]. The methacryl acid derivatives also should hardly be ionized by the effect of Ar metastable atom, and the primary structure of monomers will be maintained.

And the deposited films were analyzed by Fourier Transform Infrared (FT-IR) spectroscopy. The HOMO values of polymerized monomers were calculated by the PM3 method of MOPAC quantum chemistry computation. Further, optical emission spectrometry (OES) was employed to identify the active species in this Ar plasma jet. Based on the luminescence intensity variation of Ar plasma in the OES, the reaction mechanism of active species with monomers in this Ar plasma

jet was discussed. The Stern-Volmer plot to express the dependency of emission intensity of Ar

plasma jet on the monomer concentration was also discussed. And it was explored that the effect

of voltage and carrier gas to the polymerized film.

3.2   Experimental setup and methods

3.2.1   Experimental monomer as the precursor

In order to discuss the mechanism of the polymerization, 2-hydroxyethyl methacrylate

(HEMA), methacrylic acid (MAA) and butyl methacrylate (BMA) were chosen for methacryl

acids class polymerization experiment. The polymerized monomers were treated through reduced

pressure distillation. The properties of monomers are shown in Table 3-1 [26].

3.2.2   Atmospheric pressure non-equilibrium plasma device

The atmospheric pressure low-temperature plasma reactor used is the same as shown in Fig.

2-1. The plasma device (CAPPLAT) used in the experiment is a hand-made cold atmospheric

pressure plasma torch. The plasma torch comprises two co-axial cylindrical electrodes. With the

normal connection mode, the inner electrode (an aluminum pipe, inner diameter = 7 mm and outer

diameter = 8 mm) is connected to a high voltage power supply with a frequency of 20 kHz and

duty of 50% (Haiden Lab SBP-10K-HF). If without specific illustration, the normal connection

mode was employed in the experiments. The outer electrode (aluminum foil, width = 2 mm) is

grounded. A Laboran® silicone tube (thickness: 2 mm) acts as a dielectric barrier between the two

electrodes. The schematic illustration of the torch is the same as shown in Fig. 2-2. Further details

of the configuration of this plasma torch are provided in our previous papers [27-28].

Polymerization experiments were performed under normal conditions by applying invariable

voltage (± 3.0 kV ~ ± 4.2 kV). Ar gas was employed as the working gas. Monomer was introduced

as the additive gas into the Ar stream. The flow rates of the Ar gas were set to 3 LPM (standard liters per minute). The flow rates of additive gas were set to 0.5 ~ 2.0 LPM. All flow rates were controlled using a mass flow controller. The plasma polymerization was performed in a chamber (quartz glass container). Prior to the plasma polymerization, the air in the chamber was replaced by Ar for 5 min with 3 L/min. The deposition was carried out on a KBr disk (13 mm Φ). The deposition distance was 5 mm and the deposition time was 10 min. And in order to avoid the influence of the temperature in the ambient air, the heater band was used to keep the temperature stable (30 °C). The disk was not taken out after polymerization promptly after Ar gas was imported into the container for one minute. It should be noted that monomer was not injected directly into the Ar gas. No plasma jet was generated by such direct injection, because of the considerable quenching effect of monomers. Therefore, I added monomers to the afterglow zone of the plasma jet through a glass capillary placed at the center of the torch (see Fig. 2-2). In this case, monomers mix with the Ar plasma in the afterglow zone.

3.2.3   Ionization potential calculation

In this study, all calculations based on a Dewar and Thief's NDDO (Neglect of Diatomic Different Overlap) approximation were carried out using PM3 method [29] of a semiempirical quantum chemistry program "MOPAC" (Molecular Orbital Package, Fujitsu, SCIGRESS MO Compact 1.0.6 standard) [30].

Mo Compact builds a molecular model by mouse operation on Windows and carries out a semiempirical molecular orbital calculation. There are the effective tools which can display the result graphically. From the molecular construction, the calculation was processed seamlessly. The results of the electric dipole moment, electric charge, molecular orbital, electrostatic potential and

standard vibration is calculated by the molecular orbital calculation, which is displayed

graphically [31]. The parameter setting is shown in Fig. 3-1.

3.2.4 Optical emission spectroscopy (OES) measurement of Ar plasma jet

In addition, the optical emission spectrum (OES) measurements were performed

perpendicularly to the jet by using a multi-band plasma process monitor (MPM, Hamamatsu

Photonics C7460) for elucidating the polymerization mechanism.

The optical emission spectra of the plasma jet were collected perpendicular to the jet using an

spectrometer (spectral range of 350–950 nm) with a resolution of 0.2 nm full width at

half-maximum (FWHM); this was achieved using a personal computer equipped with relevant

software (Spectra Suite) for both driving and acquisition. Therefore, absolute irradiance of the

active species in the plasma jet was obtained. During the measurement of the optical emission

spectra, the exposure time was 100 ms. Emission intensities of the active species were collected at

an axial position of the plasma jet, through an optical fiber with a diameter of 100 μm.

3.2.5 Fourier transform infrared (FT-IR) measurement

Transmission mode for the IR spectra of the films was taken with a Fourier Transform Infrared

(FT/IR-8000, Jasco, Japan) with 64 scans at 2 cm^{-1} resolution.

3.3 Results and discussion

3.3.1 Ionization potential calculation

According to the Koopmans principle, the absolute value of HOMO (Highest occupied

molecular orbital) is the same to the ionization potential values of monomers. So I used the values

of HOMO of methacryl acid derivatives to indicate the ionization potential of monomers.

In the case of HEMA, the value of HOMO is -10.66 eV that is close to the Ar^{m} ($^{3}P_{2}$). The

methacrylic acid (MAA) and butyl methacrylate (BMA) monomers were calculated by the same method. The values of HOMO obtained from the molecular orbital calculation have been paid attention. And the calculation results of monomers were shown in Table 3-2.

3.3.2 Optical characterization of CAPPLAT Ar plasma jet

3.3.2.1 Typical optical emission spectrum

A typical optical emission spectrum of CAPPLAT Ar plasma jet in the wavelength range of 350–950 nm is shown as Fig. 2-8 in Chapter 2. It can be seen that peaks belonging to the excited Ar atoms (4p-4s transition) are predominant in this plasma jet (in the wavelength range of 690–950 nm，which was written by reaction process (1) ~ (3) in Chapter 2) [31- 36]. Emission intensities and assignments of Ar active species (in the wavelength range of 350–950 nm) detected in CAPPLAT Ar plasma jet are summarized as in Table 2-2 (the peaks of N_2 and OH is negligible, which is also written in Chapter 2).

3.3.2.2 Effect of additive gas on polymerized OES

In order to discuss the emission intensity of the plasma jet introducing the monomer, 2-hydroxyethyl methacrylate (HEMA) was chosen to represent for methacryl acids class. The OES of the plasma jet with and without monomer feed are shown in Fig. 3-2.

From the Fig. 3-2, the emission lines from the excited species do not seem to be changed even when the HEMA monomer was introduced. However, it became weaker when the monomer was introduced. This can be interpreted as the result of the energy transfer from the excited Ar to the HEMA monomer.

3.3.2.3 Effect of voltage on polymerized OES

The OES of the plasma jet with HEMA monomer by changing the voltage is shown in Fig. 3-3.

From the Fig. 3-3, the distribution of emission lines from the excited species do not seem to be changed even when the voltage was increased. But, the intensity was increased by increasing the voltage. That was because as the voltage increased the density of Ar^m was becoming larger. And the excited state of $Ar^*(4P)$ was also increased when the Ar excited from metastable state to the 4P excited state, which then lead to emission density increasing by de-excite to the ground state.

3.3.2.4 Effect of additive gas flow rate on polymerized OES

The OES of the plasma jet with HEMA monomer by changing the carrier gas flow rate is shown in Fig. 3-4. It is shown that as the carrier gas flow rate increasing the distribution of emission lines from the excited species do not seem to be changed. But, the luminous intensity became weaker when increasing the carrier gas flow rate. The reason is that the monomer has the quenching effect to the Ar gas.

3.3.2.5 Gas-phase chemistry

When only Ar was introduced from the capillary, there was almost no change in the emission intensity. However, it became weaker according to the carrier gas flow rate when the monomer was introduced. This can be interpreted as the result of the energy transfer from the excited Ar to the monomer. As the example of HEMA monomer was introduced, Ar plasma emission intensities decreased that is shown in Fig. 3-5. Therefore, when the monomer was introduced as the precursor into the Ar plasma, I suppose reaction (4) were happened possibly that showed below,

$$Ar^m + M \text{ (monomer)} \rightarrow Ar^0 + M^* \tag{4}$$

Where, Ar^0 indicates the ground state of Ar; Ar^m indicates the metasable state of Ar; M^* indicates the excited state of monomer. When monomer was introduced, reaction (4) occurred, which will decrease the quantity of Ar metastable. Consequently, the emission intensities of

excited Ar atoms weakened since the reaction (2) was restrained.

When the energy is transferring to the monomer, the concentration of Ar^m has the relationship that showed in reaction (5).

$$\frac{d[Ar^m]}{dt} = k_0[Ar^m] + k_q[Ar^m][M]$$

$$= (k_0 + k_q[M])[Ar^m] \tag{5}$$

And then, the concentration of Ar^m will become to $k_0 / (k_0 + k_q[M])$ times to that when monomer is not introduced.

In other words, I_0 represents for luminescent intensity when monomer is not introduced, I represents for luminescent intensity when monomer is introduced, as a result:

$$\frac{I_0}{I} = \frac{k_0[Ar^m]}{k_0[Ar^m] \bullet k_0 / (k_0 + k_q[M])} = \frac{k_0}{k_0^2 / (k_0 + k_q[M])} = \frac{k_0 + k_q[M]}{k_0} = 1 + \frac{k_q}{k_0}[M] \tag{6}$$

Basing on the relationship as shown in equation (6), when monomer is introduced to the Ar plasma, we can use the Stern-Volmer plot to express the dependency of emission intensity on the monomer concentration. The results obtained for HEMA system is shown in Fig. 3-6. It is obvious that the value of I_0 / I increases with the monomer feed ratio.

3.3.3   Chemical Structure of the Plasma-Polymerized Films by FT-IR

3.3.3.1   The relationship between carrier gas flow rate and monomer supply rate

In the experiment, it is discussed that the relationship between monomer supply rate to the plasma and the variation of the carrier gas flow rate, which are shown in Fig. 3-7 and Fig. 3-8 for the monomer of HEMA and MAA separately. In the unit time, the supply rate was calculated dependence on the gas flow rate. From the Fig. 3-7 and Fig. 3-8, it is confirmed that the actually supply rate increased accompanying with the carrier gas flow rate.

3.3.3.2 The relationship between monomer supply rate and yield of the polymerized film

By the measurement of FT-IR, the absorbance (Abs) results of polymerized film were obtained. And it is thought that in the same polymerized film, the yield of the production becomes bigger in the meantime of the Abs is higher. So taking the Abs of the C=O peak for the example in the HEMA and MAA FT-IR results, the relationship dependence on the carrier gas flow rate is shown in Fig. 3-9 and Fig. 3-10 separately.

When the carrier gas flow rate is becoming bigger, the absorbance of C=O in the polymerized film becomes higher. From the reasons above, it is understood when the carrier gas flow rate becomes bigger, the monomer supply rate becoming larger followed by the yield of the polymerized film increasing.

3.3.3.3 Plasma-polymerized films by FT-IR

In order to discuss the polymerized HEMA film by the plasma whether or not maintaining the primary structure as the conventional polymerized HEMA film, I also used the free radical polymerization method to obtain conventional PHEMA. The polymerization of HEMA was performed in a 10% monomer solution in deionized water at 70 ℃, using potassium (KPS) initiator. The synthesis was carried out in a three-necked flask equipped with a mechanical stirrer, using a water bath for temperature control. Before heating, the N_2 gas was introduced to the reaction mixture with continuous stirring for 40 minutes. The synthesis time was 3 h. After synthesis, the reaction mixture was cooled and the reaction products were washed out with deionized water and additionally methanol for three times separately. And the products were desiccated in the vacuum oven for 10 h at 50 ℃.

The FTIR spectrums of conventional polymerized HEMA and plasma polymerized HEMA are

shown in Fig. 3-11.

As is shown in Fig. 3-11, it is obviously that the peak of C=C (1640 cm^{-1}) bond in the monomer disappeared in both spectrums which confirmed that the additional polymerization proceeded. On the other hand, it is obvious that HEMA has been polymerized by the plasma with keeping its primary structure since the characteristic peaks of OH (around 3500 cm^{-1}), CH$_3$, CH$_2$ (2962 cm^{-1}, 2899 cm^{-1}), C-O-C (1075 cm^{-1} – 1020 cm^{-1}) and C=O (1733 cm^{-1}) in the monomer have been maintained. Therefore, it is conclude that polymerization of HEMA monomer with maintaining the primary structure was succeeded by using the plasma equipment.

3.3.3.4 Effect of voltage on plasma-polymerized films by FT-IR

The polymeric FTIR spectrum of HEMA with changing applied voltage is shown in Fig. 3-12. As mentioned above, as the voltage increased the density of Ar^m was also increased. The rate of polymerization was also speed up by the effect of the Ar^m quantity. In addition, the structure of the product did not change even when adjusting the voltage as the variation of changing the carrier gas flow rate. Generally, a higher applied voltage leads to stronger plasma, in turn leads to a faster deposition rate and a thicker film at a certain deposition time. The results showed in Fig. 3-12 indicate the deposition rate increased as the applied voltage increased and the primary structure was retained, too.

3.3.3.5 Effect of monomer flow rate on plasma-polymerized films by FT-IR

The polymeric FTIR spectrum of HEMA with changing HEMA flow rate is shown in Fig. 3-13.

The structure of the product did not change even when adjusting the carrier gas rate. The difference in absorption intensity could be attributed to the difference in the thickness of films.

The larger monomer feed ratio will lead to the faster deposition rate as well if the plasma intensity is sufficient for the polymerization of the introduced monomer. As the same effect with the voltage mentioned, the results showed in Fig.3-13 indicate the deposition rate increased as the monomer feed ratio increased. In spite of changing the carrier gas rate, it is also confirmed that primary structure was maintained through polymerization.

The plasma polymerized MAA film was also discussed with the conventional polymerized MAA film by comparing the primary structure. The polymerization of MAA was performed in a 40% monomer solution in acetone at 60 ℃, using 2, 2` - azobis (isobutyronitrile) (AIBN) initiator (0.2% with respect to the monomer weight). The synthesis was carried out in a three-necked flask equipped with a mechanical stirrer, using a water bath for temperature control. Before heating, the N_2 gas was introduced to the reaction mixture with continuous stirring for 40 minutes. The synthesis time was 5 h. PMAA was precipitated from the acetone solution in the course of the synthesis. And using decantation method with acetone for three times, residual monomer was washed out by acetone. The products were desiccated in the vacuum oven for 10 h at 80 ℃.

The FT-IR spectrums of conventional polymerized MAA and plasma polymerized MAA are shown in Fig. 3-14, which indicated that MAA monomer was polymerized successfully with maintaining the primary structure by the CAPPLAT equipment.

And, the FT-IR spectra of MAA deposited films are shown in Fig. 3-15. There was no effect to the structure of the deposited films by changing the carrier gas rate and voltage, which coinciding with the same tendency of HEMA polymerized films. And the C=C bond peak (1640 cm^{-1}) was disappeared. The specific C=O bond (1715 cm^{-1}), CH_3, CH_2 (2984 cm^{-1}, 2966 cm^{-1}), and OH band (around 3500cm^{-1}) were appeared observably.

The plasma polymerized BMA has the same functional group with the conventional polymerized BMA, which are shown in Fig. 3-16. The free radical polymerization method used for the conventional polymerized BMA was the same used for the HEMA polymerization.

Comparing with the conventional PBMA, BMA monomer was polymerized successfully with maintaining the primary structure by the CAPPLAT equipment.

The FT-IR spectra of BMA deposited films are shown in Fig. 3-17. As the HEMA, the stable polymerized structure was obtained. It is confirmed that the polymerization was successfully processed because of the C=C peak (1641 cm^{-1}) disappeared. The peaks of C=O bond (1736 cm^{-1}) and CH_3, CH_2 (2966 cm^{-1}, 2878 cm^{-1}) were showed clearly.

Through the results mentioned above, the FT-IR results were consistent with the MOPAC molecular calculation result, which speculated that it could be maintained the primary structure of HEMA, MAA and BMA in the polymerization process. Then, it is concluded that the methacryl acid and its derivatives would be polymerized.

3.4 Conclusions

In this study, in order to ascertain the working hypothesis postulated in the former chapter, methacrylic monomers were polymerized with atmospheric pressure non-equilibrium Ar plasma jet.

Through the HOMO orbital calculation by the PM3 for HEMA monomer, the value of HOMO was found to be -10.66 eV, which was close to the Ar^m (11.55 eV). The HOMO values of MAA and BMA monomer were estimated as -10.61 eV and -10.62 eV, respectively. The ionization potential values of monomers were close to the Ar^m energy and it was supposed that the methacrylic monomers were difficult to be ionized.

OES study only showed that the energy was transferred from Ar^m to the monomers. And the Stern-Volmer plot to express the dependency of emission intensity of Ar plasma jet on the monomer concentration became linear indicating that the energy transfer from Ar^m to the monomer took place quantitatively. When the voltage increased, the luminescence intensity and the density of Ar metastable atom were also increased, which gained a higher reaction rate of polymerization. And similarly, increasing the carrier gas flow rate, the reaction rate of polymerization was increased.

The FT-IR analyses confirmed that plasma-polymerized HEMA, MAA and BMA kept their primary structure of monomer molecules unlike styrene which ionized by the Ar plasma, which proved the working hypothesis postulated mentioned above

Therefore, it was strongly suggested that the functional groups composed of monomer could be retained when the polymerization was proceeded for the monomer of which ionization potential is close to the energy of Ar^m.

References

[1] S. I. Rapaport, S. B. Ames, S. Mikkelsen, J. R. Goodman, N. Engl. J. Med., 263, 278-282 (1960).

[2] R. Prat, Y. J. Koh, Y. Babukutty, M. Kogoma, S. Okazaki, M. Kodama, Polymer, 41, 7355-7360 (2000).

[3] T. P. Kasih, S. Kuroda, H. Kubota, Plasma Processes and Polymers , 4(6), 648-653 (2007).

[4] M. Bashir, J. M. Rees, W. B. Zimmerman, DOI 10.1016/j.surfcoat.2013.01.041 (2013).

[5] A. F. Bublievskii, A. A. Galinovskii, A. V. Gorbunov, S. A. Zhdanok, V. A. Koval, L. I. Sharakhovskii, G. V. Dolgolenko, D. S. Skomorokhov, J. Eng. Phys. Thermophys., 79, 629 (2006).

[6] V. Poenariu, M.R. Wertheimer, R.Bartnikas, Plasma Process. Polym., 3, 17 (2006).

[7] http://www.cresur.com

[8] A. Kuwabara, S. Kuroda, H. Kubota, Plasma Sources Sci. Technol., 15, 328 (2006).

[9] T. P. Kasih, S. Kuroda, H. Kubota, Chem. Vap. Depos., 13, 1 (2007).

[10] A. Kuwabara, S. Kuroda, H. Kubota, Plasma Sci. Technol., 9, 181 (2007).

[11] A. Kuwabara, S. Kuroda, H. Kubota, Plasma Chem. Plasma Process., 28, 263 (2008).

[12] T. P. Kasih, S. Kuroda, H. Kubota: Plasma Processes and Polymers., 4(6), 648-653 (2007).

[13] J. P. Montheard, M. Chatzopoulos, D. Chappard, JMS-Rev. Macromol. Chem. Phys., C32, 1 (1992).

[14] B. D. Ratner, A. S. Hofman, Polym. Sci. Technol., 7, 159 (1975).

[15] C. G. Beddows, M. H. Gil, J. T. Guthrie, J. Appl. Polym. Sci., 35, 135 (1988).

[16] J. O. Karlsson, P. Gatenholm, Polymer, 38, 4727 (1997).

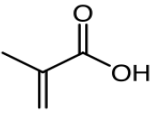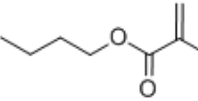[17] H. Demircioglu, H. Beyenal, A. Tanyolac, N. Hasirci, Polym. Int., 35, 321 (1994).
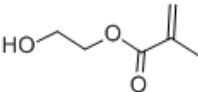
[18] A. B. Clayton, T. V. Chirila, X. Lou, Polym. Int., 44 201 (1997).

[19] A. Denizli, R. Say, S. Patir, M. Y. Arica, React Funct. Polym., 43, 17 (2000).

[20] E. H. Ibrahim, A. Denizli, S. Bektas, O. Genc, E. Piskin, J. Chromatogr., B720, 217 (1998).

[21] A. Zubaidi, T. Hirotsu, J. Appl. Polym. Sci., 61, 1579 (1996).

[22] M. Morra, E. Occhiello, F. Garbassi, J. Adhes., 46, 39 (1994).

[23] J. Folkman, A. Moscona, Nature. 273, 345 (1978).

[24] M. Y. Arica, S. Senel, N. G. Alaeddinoglu, E. Patir, J. Chromatogr., B720, 217 (1998).

[25] M. Ukai, J. Mass Spectrom. Soc. Jpn. 57 (6), 393 (2009).

[26] http://www.chemindustry.com/apps/chemicals

[27] X. Fei, Y. Kondo, X. Qian, S. Kuroda, T. Mori, K. Hosoi, Key Engineering Materials., 596, 65-69 (2014).

[28] J. Yan, Y. Kondo, X. Qian, X. Fei, K. Hosoi, T. Mori, S. Kuroda, Applied Mechanics and Materials., 423-426, 537-540 (2013).

[29] J. J. P. Stewart: Journal of Computer-Aided Molecular Design., 4(1), 1-103 (1990).

[30] R. M. Metzger, Acc. Chem. Res., 32(11), 950-957 (1999).

[31] SCIGRESS Mo Compact 1.0 User Guide.

[32] Y. Harada, S. Masuda, H. Ozaki, Chem. Rev., 97, 1897-1952 (1997).

[33] A. F. Bublievskii, A. A. Galinovskii, A. V. Gorbunov, S. A. Zhdanok, V. A. Koval, L. I. Sharakhovskii, G. V. Dolgolenko, D. S. Skomorokhov, J. Eng. Phys. Thermophys., 79, 629 (2006).

[34] V. Poenariu, M. R. Wertheimer, R. Bartnikas, Plasma Process. Polym., 3, 17 (2006).

[35] J. Kuba, L. Kucera, F. Plzak, M. Dvorak, J. Mraz, Coincidence Tables for Atomic Spectroscopy, Elsevier Publishing Company (1965).

[36] K. Hiraoka, S. Fujimaki, S. Kambara, H. Furuya and S. Okazaki, Rapid Commun. Mass Spectrom., 18, 2323-2330 (2004).

[37] S. Tsujiyama and N. Takada, Japanese Society of Mushroom Science and Biotechnology. 12 (2), 85 (2004).

[38] M. Ishihara and S. Fujisawa, Dental Materials Journal 28 (1), 113 (2009).

Table 3-1 The properties of polymerized monomer list

Monomer	Molecular Formular	Chemical Formular	Molecular Weight (g/mol)	Density (g/cm^3)	Boiling Point (℃)
Methacrylate **2-Hydroxyethyl** (HEMA)	$C_6H_{10}O_3$		130.14	1.073	205
Methacrylic **Acid** (MAA)	$C_4H_6O_2$		86.09	1.02	159-163
Methacrylate **Butyl** (BMA)	$C_8H_{14}O_2$		142.2	0.89	162-165

Table 3-2 The comparison between the calculated results of HOMO by the PM3 method of MOPAC and the calculated results from the reference

Monomer	Calculated HOMO values by the PM3 of MOPAC	HOMO values from the reference	Ionization Potential (GFG Instrumentation Database)
MMA	-10.559 eV	-10.548 eV— Ref. 38	9.70 eV
Styrene	-9.131 eV	-9.470 eV—Ref. 37	8.47 eV
HEMA	-10.663 eV	-10.573 eV—Ref. 38	No data
MAA	-10.611 eV	-11.066 eV—Ref. 38	No data
BMA	-10.623 eV	-10.530 eV—Ref. 38	No data
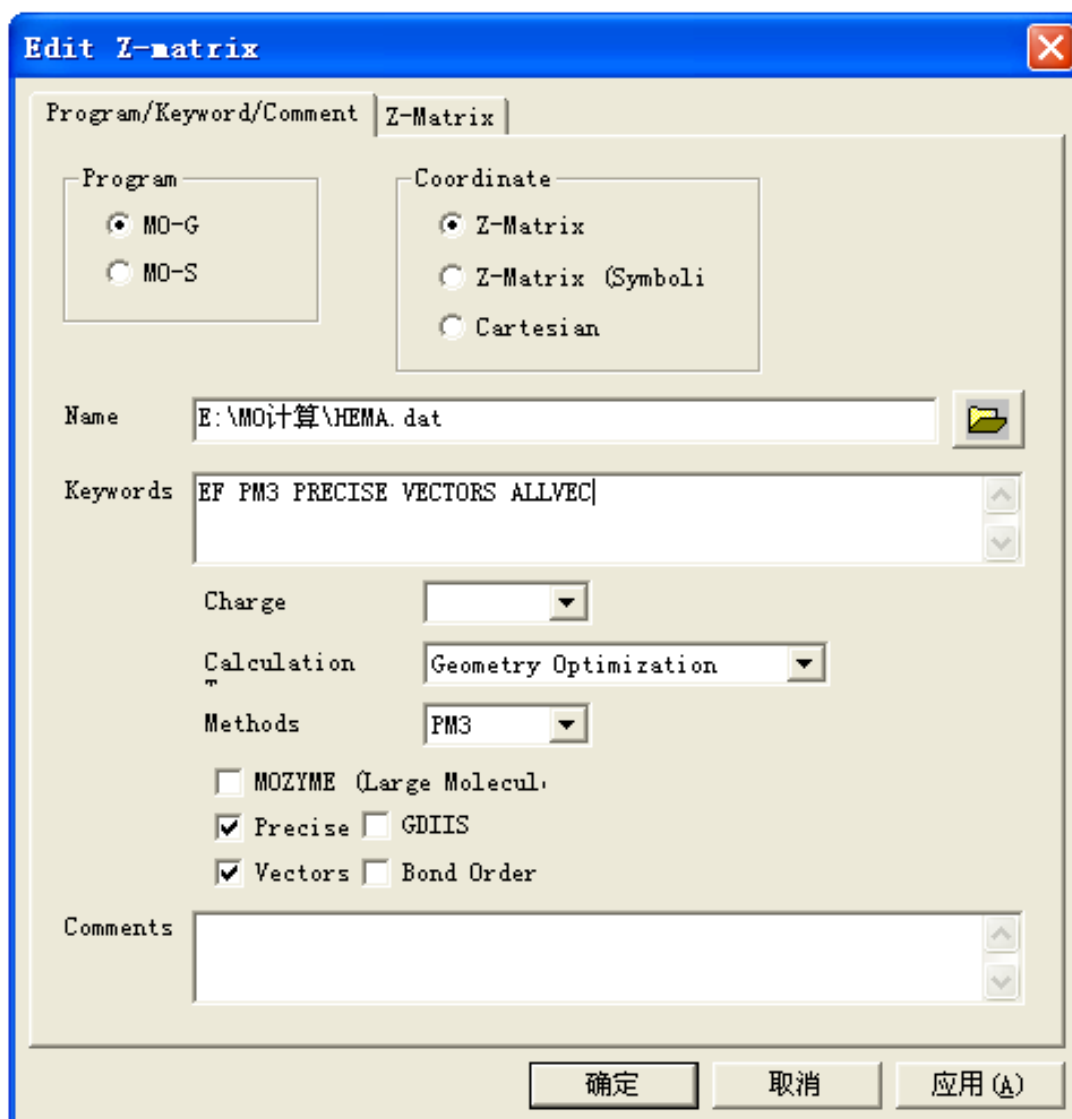
Fig. 3-1 Parameter Setting of MOPAC molecular orbital calculation.
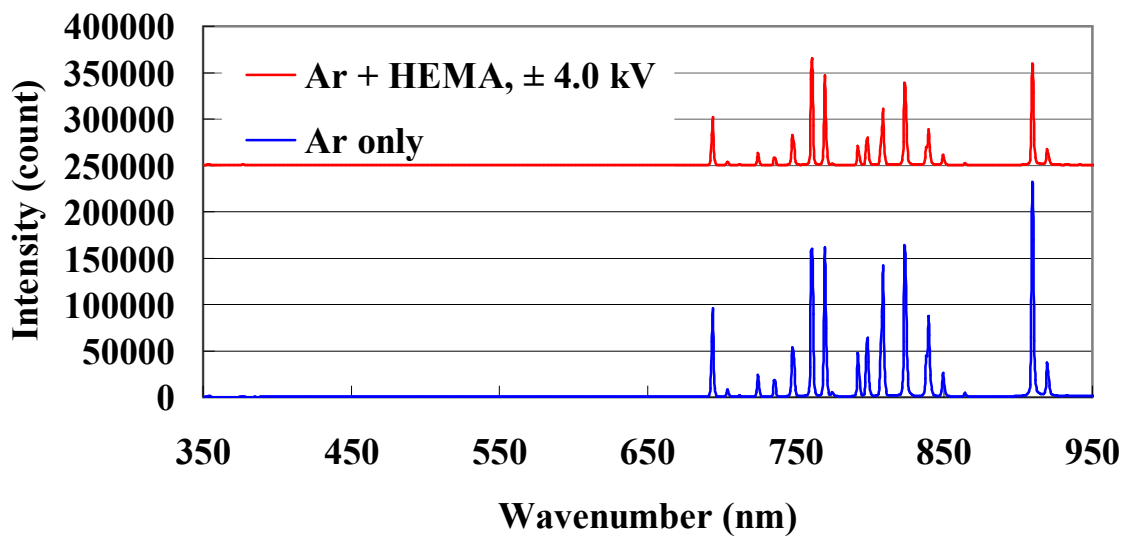
Fig. 3-2 Optical emission spectra of plasma jet with and without HEMA monomer measured at a distance of 5 mm from the end of torch. Discharge conditions: pure Ar discharge at a flow rate of 3 L/min, carrier gas flow 1.5 L/min, dielectric thickness of 2 mm, nominal applied voltage of ± 4.0 kV (peak to peak) with 50% duty cycle, discharge frequency of 20 kHz.
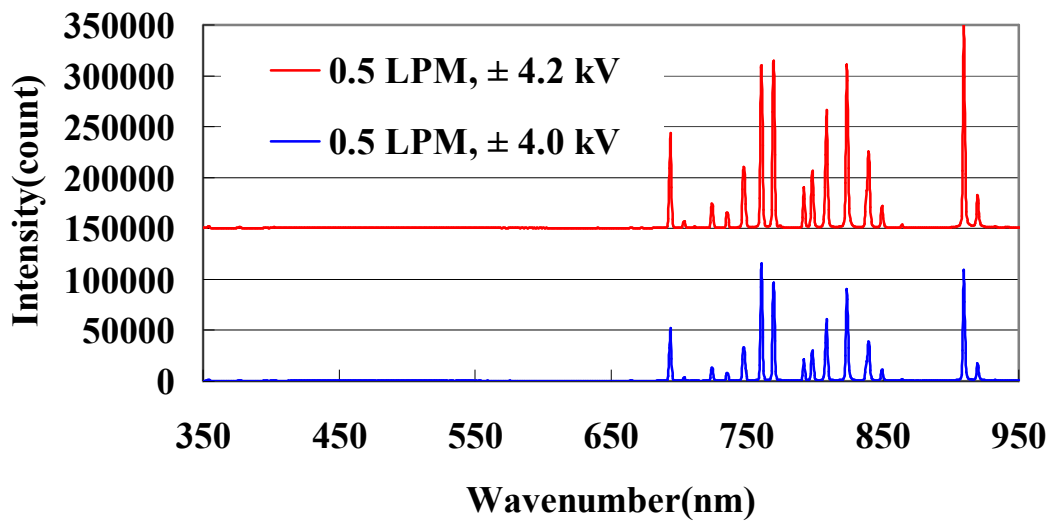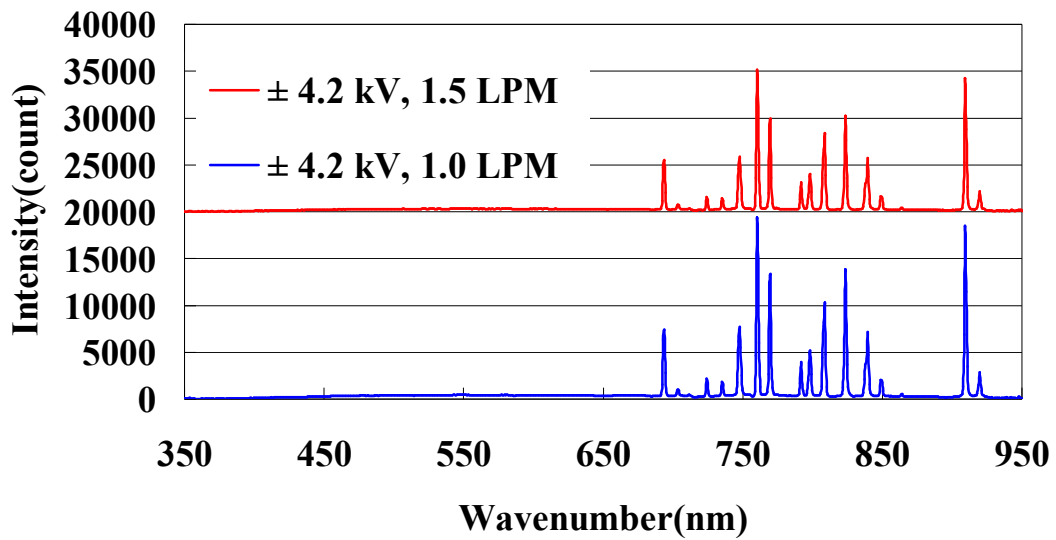
**Fig. 3-3 Optical emission spectra of plasma jet with HEMA monomer measured at a distance of 5 mm from the end of torch. Discharge conditions: pure Ar discharge at a flow rate of 3 L/min, carrier gas flow 0.5 L/min, dielectric thickness of 2 mm, nominal applied voltage of ± 4.0 kV and ± 4.2 kV (peak to peak) with 50% duty cycle, discharge frequency of 20 kHz.**

Fig. 3-4 Optical emission spectra of plasma jet with HEMA monomer at different carrier gas flow measured at a distance of 5 mm from the end of torch. Discharge conditions: pure Ar discharge at a flow rate of 3 L/min, carrier gas flow 1.0 L/min and 1.5 L/min, dielectric thickness of 2 mm, nominal applied voltage of ± 4.2kV (peak to peak) with 50% duty cycle, discharge frequency of 20 kHz.
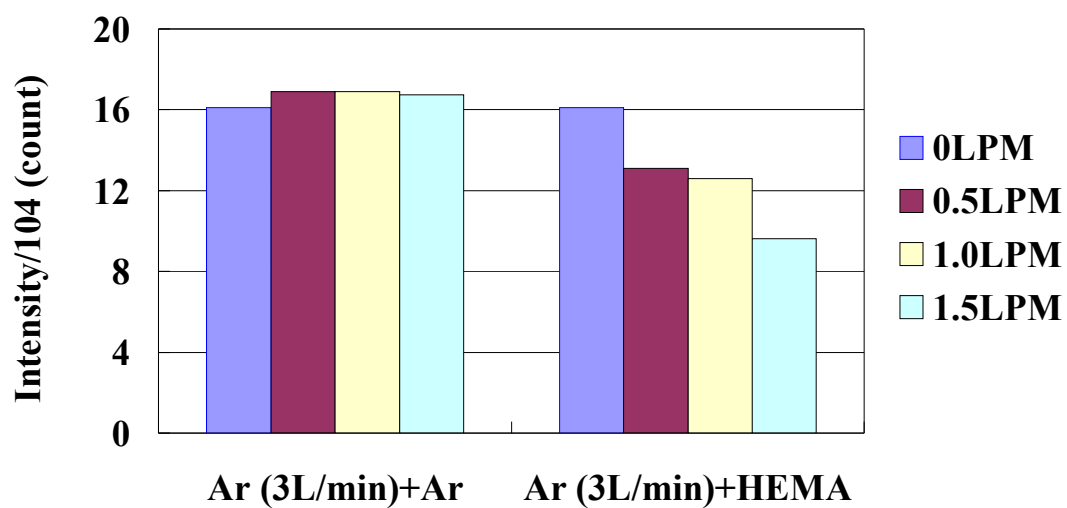
Fig. 3-5 Luminescent intensity of Ar (769 nm) luminescent species.
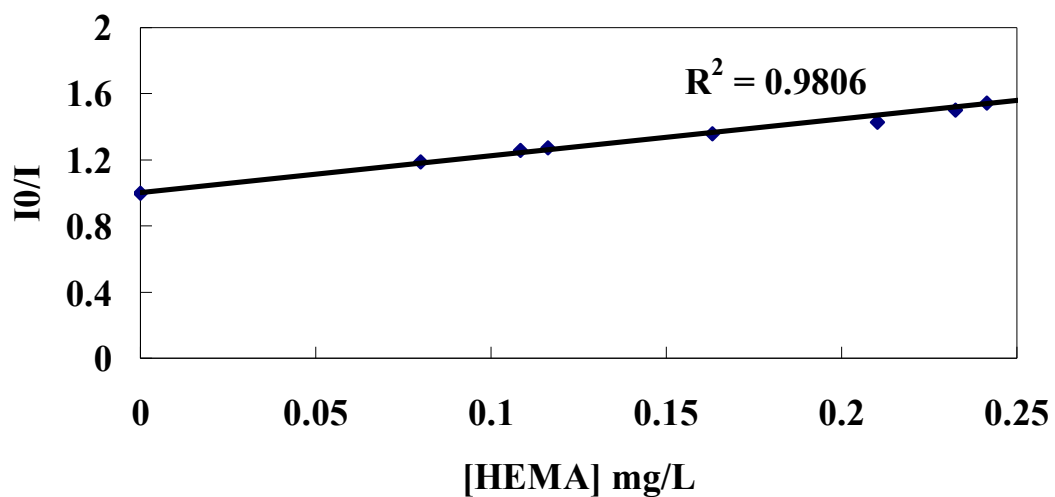
Fig. 3-6 Stern-Volmer plot for the emission intensity from Ar* at 769 nm against the monomer feed ratio. Plasma voltage = ± 4 kV (peak to peak).
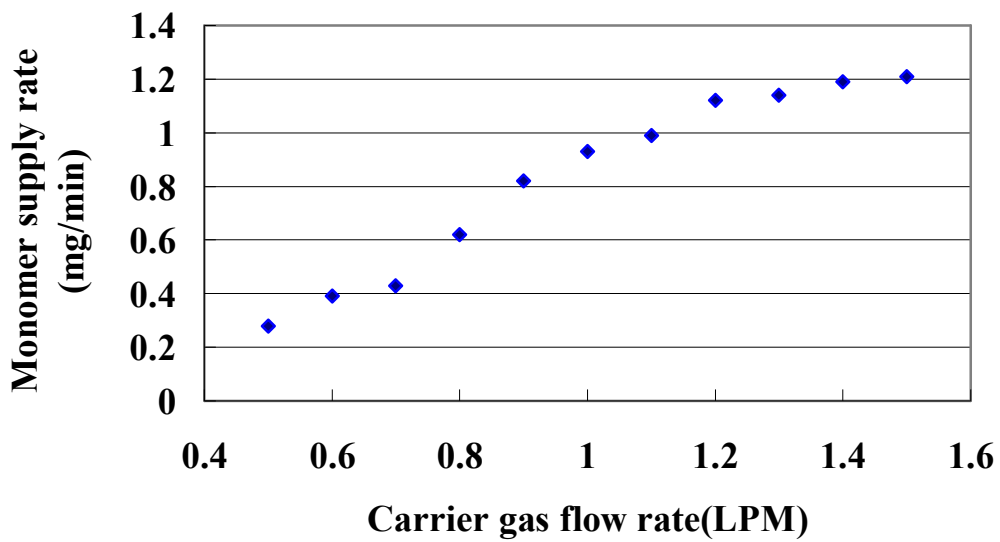
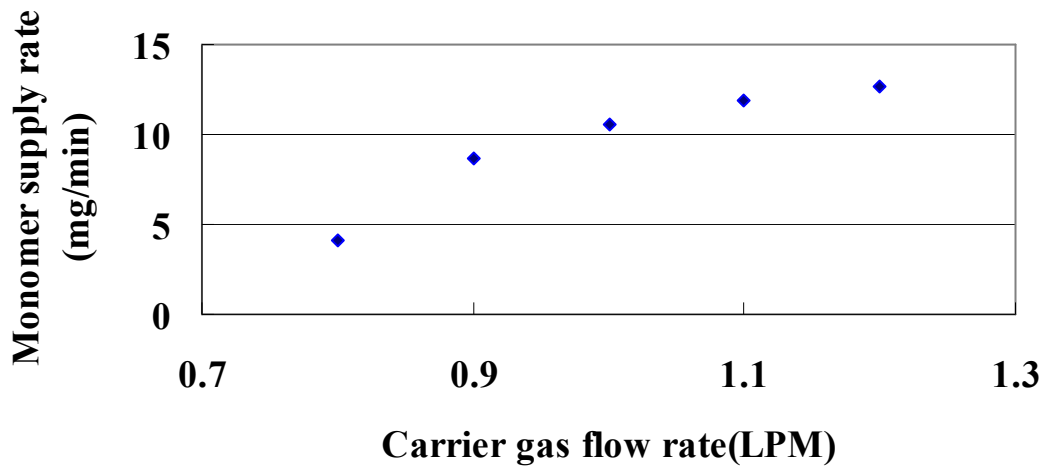**Fig. 3-7 The relationship between carrier gas flow rate and supply rate for HEME monomer.**
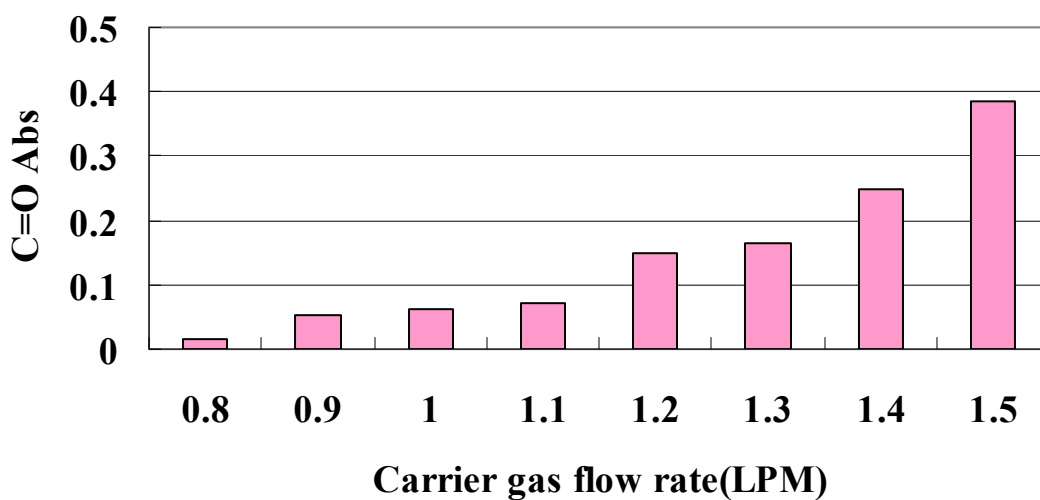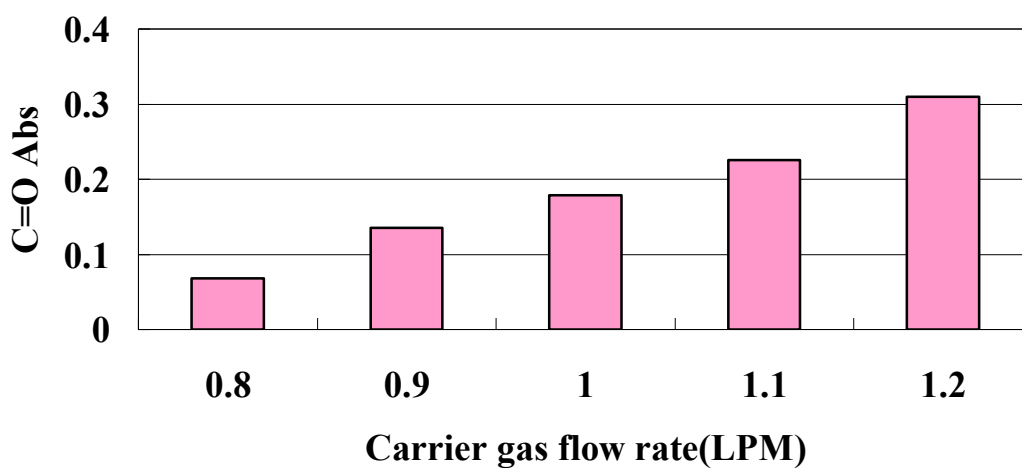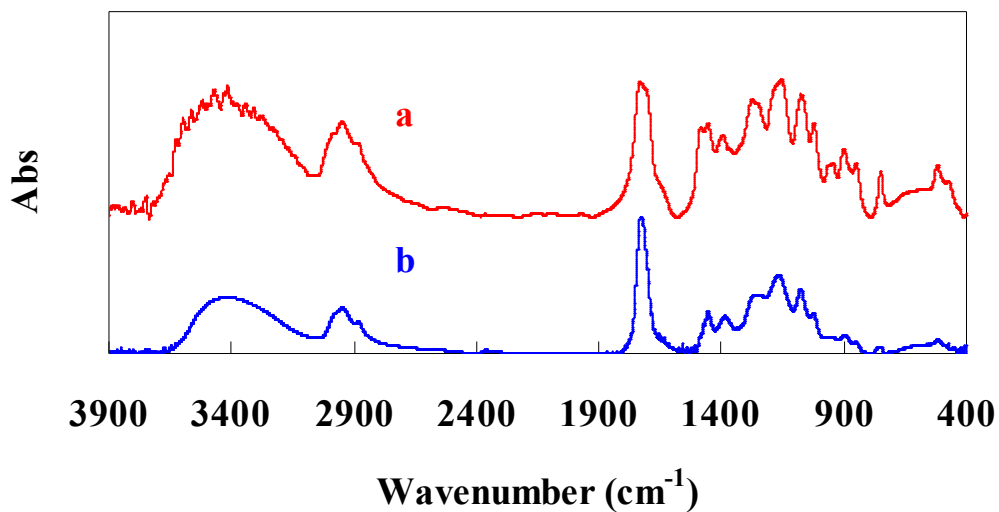

Fig. 3-8 The relationship between carrier gas flow rate and supply rate for MAA monomer.

Fig. 3-9 The absorbance (Abs) of C=O dependence on the carrier gas flow rate for HEMA monomer at the voltage of ± 4.0 kV (peak to peak).


Fig. 3-10 The absorbance (Abs) of C=O dependence on the carrier gas flow rate for MAA monomer at the voltage of ± 4.0 kV (peak to peak).

Fig. 3-11 The FT-IR spectrums of conventional polymerized HEMA (a) and plasma polymerized HEMA film (b). Discharge conditions: pure Ar discharge at a flow rate of 3 L/min, carrier gas 1.5 LPM, dielectric thickness of 2 mm, nominal applied voltage of ± 4.2 kV (peak to peak) with 50% duty cycle, discharge frequency of 20 kHz.
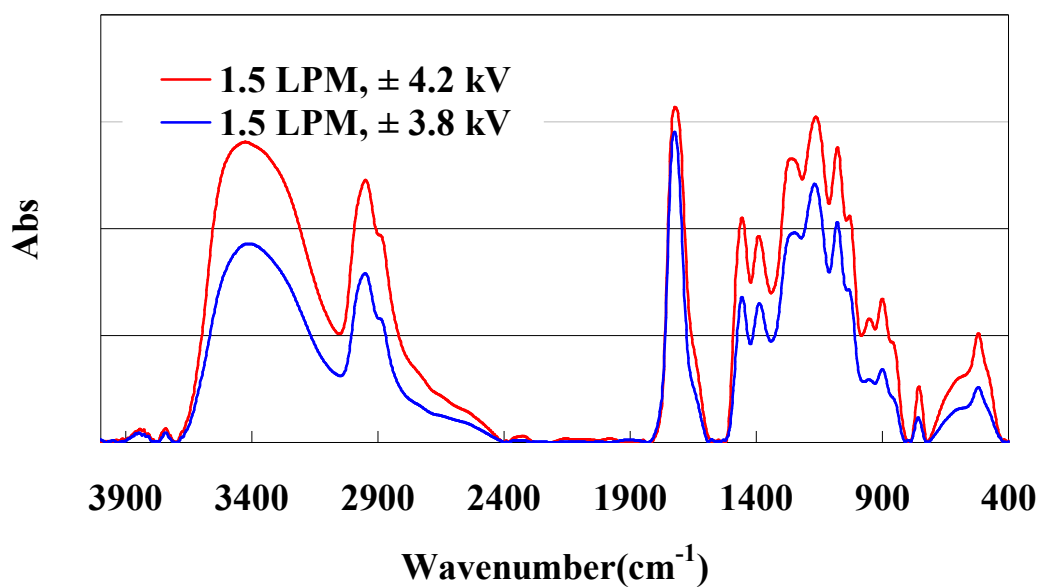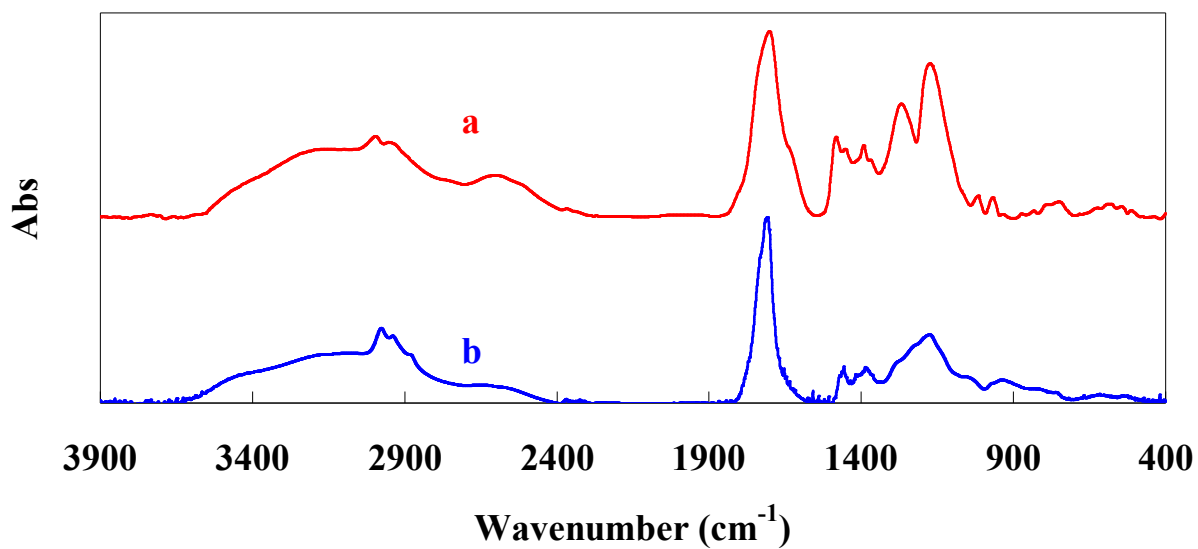
Fig. 3-12 The polymeric IR spectrum of HEMA film by changing the voltage. Discharge conditions: pure Ar discharge at a flow rate of 3 L/min, carrier gas 1.5 LPM, dielectric thickness of 2 mm, nominal applied voltage of ± 3.8 kV and ± 4.2 kV (peak to peak) with 50% duty cycle, discharge frequency of 20 kHz.
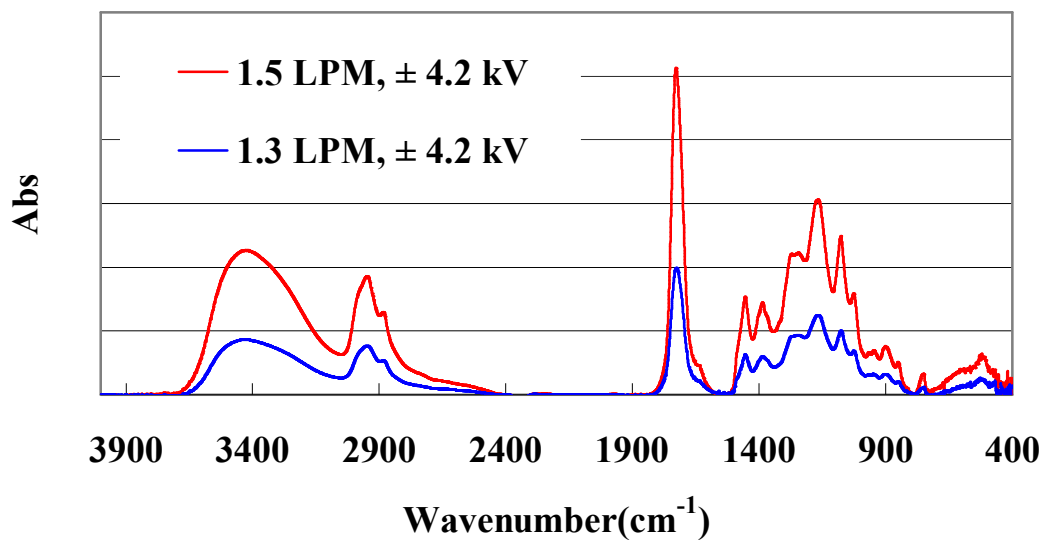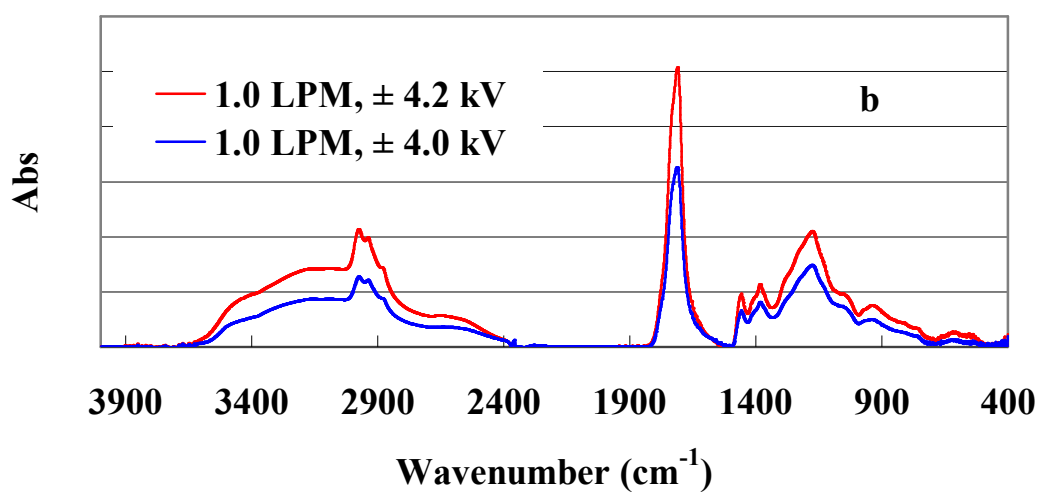
Fig. 3-13 The polymeric IR spectrum of HEMA film by changing the carries gas flow rate.

Discharge conditions: pure Ar discharge at a flow rate of 3 L/min, carrier gas 1.3 LPM and

1.5 LPM, dielectric thickness of 2 mm, nominal applied voltage of ± 4.2 kV (peak to peak)

with 50% duty cycle, discharge frequency of 20 kHz.

Fig. 3-14 The FT-IR spectrums of conventional polymerized MAA (a) and plasma polymerized MAA film (b). Discharge conditions: pure Ar discharge at a flow rate of 3 L/min, carrier gas 1.0 LPM, dielectric thickness of 2 mm, nominal applied voltage of ± 4.0 kV (peak to peak) with 50% duty cycle, discharge frequency of 20 kHz.

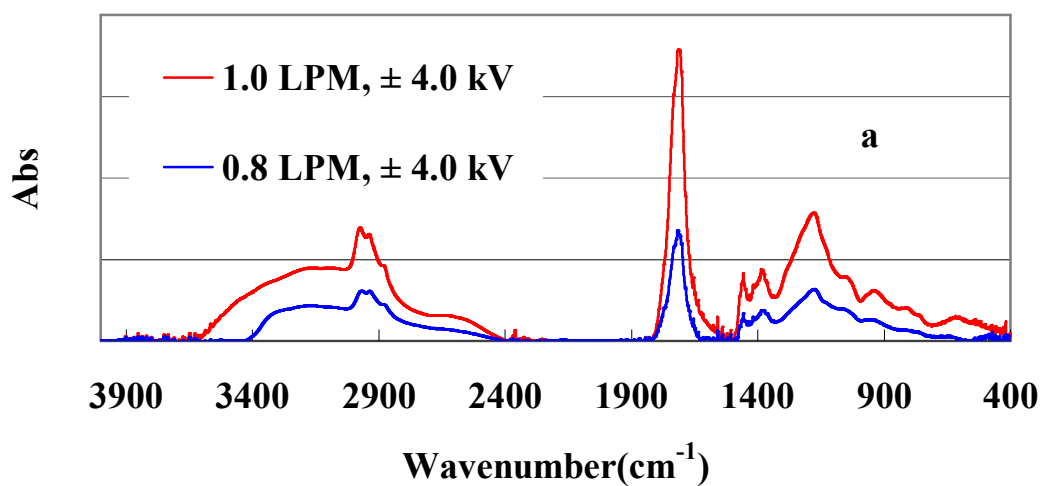**Fig. 3-15 The polymeric IR spectrum of MAA film by changing the carrier gas ratio (a) and voltage (b). Discharge conditions: dielectric thickness of 2 mm, pure Ar discharge at a flow rate of 3 L/min, carrier gas 0.8 L/min and 1.0 L/min, nominal applied voltage of ± 4.0 kV and ± 4.2 kV (peak to peak) with 50% duty cycle, discharge frequency of 20 kHz.**
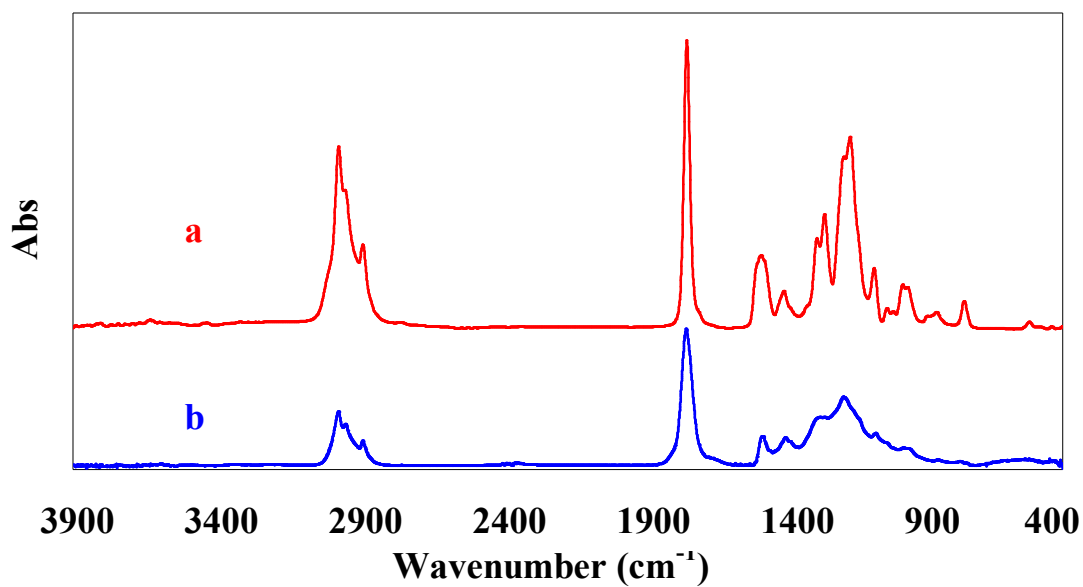
Fig. 3-16 The FT-IR spectrums of conventional polymerized BMA (a) and plasma polymerized BMA film (b). Discharge conditions: pure Ar discharge at a flow rate of 3 L/min, carrier gas 1.2 L/min, dielectric thickness of 2 mm, nominal applied voltage of ± 4.2 kV (peak to peak) with 50% duty cycle, discharge frequency of 20 kHz.
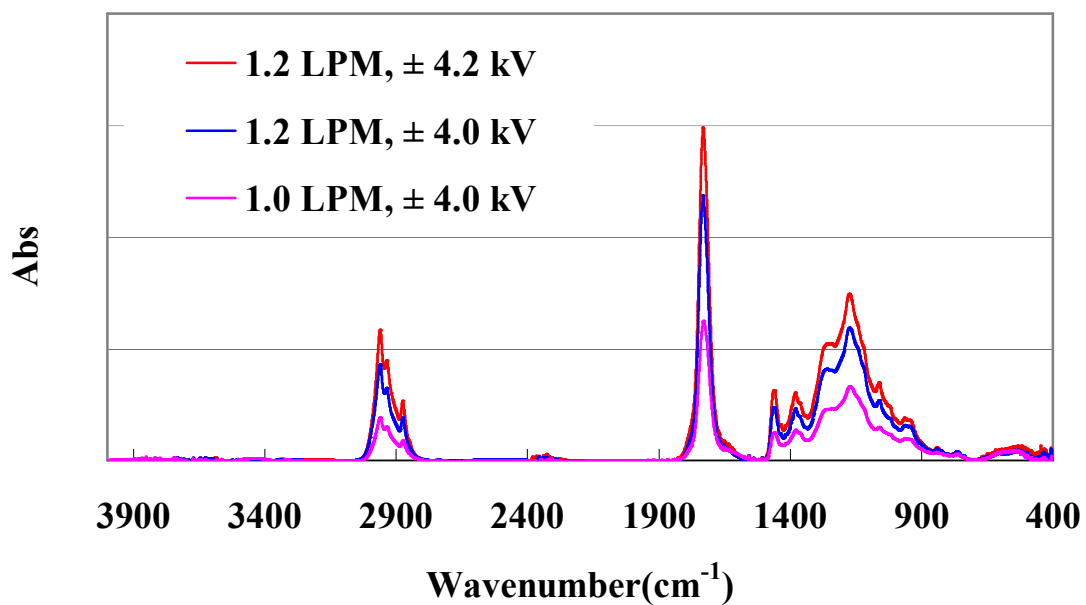
Fig. 3-17 The polymeric IR spectrum of BMA film by changing the carrier gas ratio and voltage. Discharge conditions: dielectric thickness of 2 mm, pure Ar discharge at a flow rate of 3 L/min, carrier gas 1.0 L/min and 1.2 L/min, nominal applied voltage of ± 4.0 kV and ± 4.2 kV (peak to peak) with 50% duty cycle, discharge frequency of 20 kHz.

Chapter 4 Polymerization of Maleic Anhydride Induced by Atmospheric Pressure Non-Equilibrium Plasma Jet

4.1 Introduction

Atmospheric pressure plasma jet polymerization can be used to deposit thin films showing a variety of chemical structures and properties, which are dependent on the experimental conditions (such as input power, gas composition and substrates position).

Maleic anhydride (MA) is of particular interest for the synthesis of functional organic thin films which contains two types of reactive site: the anhydride functionality and the C=C double bond. It can participate in a variety of reactions including: the Diels-Alder reaction [1], attack on allylic hydrogen atoms to form asymmetric carbon centers [2], photochemical reactions [3-5].

It has been assumed that MA polymerizes with much difficulty because of high steric hindrance resulting from disubstitution. In contrast, MA is a powerful electron acceptor, readily proceeding co-polymerization with electron donors, such as vinyl acetate, styrene, N-vinylpyrrolidone, 2-vinylnaphalene and so on [6-14]. Currently, however, MA was photographed onto low density polyethylene substrates at temperatures above the melting point of MA [15].

Schiller et al. [16] investigated plasma-assisted polymerization of maleic anhydride under different experimental conditions. The data in the study presented confirm that pulsed plasma polymerization of maleic anhydride offers possibilities to synthesis unique polymeric films. And the combined information from FT-IR, XPS, electrochemistry, and contact angle measurements demonstrate that with decreasing duty cycle (or average input power) a polymer network is formed with an increasing abundance of anhydride groups which is accompanied by decreased

cross-linking.

In the study, the non-equilibrium atmospheric pressure Ar plasma was applied to the polymerization of maleic anhydride (MA). Since the ionization energy of MA is 10.5 eV that is close to the energy of Ar^m, the polymerization mechanism assumed in the former chapters suggested it possible for MA to be polymerized. The deposited films were analyzed by using Fourier transform infrared spectroscopy (FT-IR). The intensity of optical emission spectroscopy (OES) of the plasma jet was found to become weaker when the monomer was introduced into the jet. Through the PM3 method of MOPAC quantum chemistry computation, the SOMO and SOMO' energy gap of MA and the electron density of each atom in different excited states are calculated. According to the calculation of excited state orbital charge distribution, I attempted to discuss the monomer electronic states induced by the Ar metastable atom, and the polymerization mechanism will be elucidated in order to understand polymerization process combining with polymerization kinetics.

4.2   Experimental setup and methods

4.2.1   Experimental monomer as the precursor

In order to discuss the mechanism of the polymerization, maleic anhydride was chosen for anhydride class polymerization experiment. The maleic anhydride monomer was treated through reduced pressure distillation before polymerization. The properties of monomer are showed in Table 4-1 [17].

4.2.2   Atmospheric pressure non-equilibrium plasma device

The atmospheric pressure low-temperature plasma reactor was used as shown in Fig. 2-1 and Fig. 2-2. Further details of the configuration of this plasma torch are provided in our previous

papers [18-19].

Polymerization experiments were performed under normal conditions by applying invariable voltage (± 3.8 kV~± 4.3 kV). Ar gas was employed as the working gas. Monomer was introduced as the additive gas into the Ar stream. The flow rates of the Ar gas were set to 3 LPM (standard liters per minute). The flow rates of additive gas were set to 0.5 ~ 2.0 LPM. All flow rates were controlled using a mass flow controller. The plasma polymerization was performed in a chamber (quartz glass container). Prior to the plasma polymerization, the air in the chamber was replaced by Ar for 5 min with 3 L/min. The deposition was carried out on a KBr disk (13 mm Φ). The deposition distance was 5 mm and the deposition time was 10 min. The disk was not taken out after polymerization promptly after Ar gas was imported into the container for one minute. It should be noted that monomer was not injected directly into the Ar gas. No plasma jet was generated by such direct injection, because of the considerable quenching effect of monomers. Therefore, I added monomers to the afterglow zone of the plasma jet through a glass capillary placed at the center of the torch (see Fig. 2-2). In this case, monomers mix with the Ar plasma in the afterglow zone.

4.2.3 Optical emission spectroscopy (OES) measurement

In addition, the optical emission spectrum (OES) measurements were performed perpendicularly to the jet by using a multi-band plasma process monitor (MPM, Hamamatsu Photonics C7460) for elucidating the polymerization mechanism.

The optical emission spectra of the plasma jet were collected perpendicular to the plasma jet as spectral range of 350–950 nm with a resolution of 0.2 nm full width at half-maximum (FWHM); this was achieved using a personal computer equipped with relevant software (Spectra Suite) for

both driving and acquisition. Therefore, absolute irradiance of the active species in the plasma jet was obtained. During the measurement of the optical emission spectra, the exposure time was 500 ms. Emission intensities of the active species were collected at an axial position of the plasma jet, through an optical fiber with a diameter of 100 μm.

4.2.4   Fourier transform infrared (FT-IR) measurement

Transmission mode for the IR spectra of the films was taken with a Fourier Transform Infrared (FT/IR-8000, Jasco, Japan) with 64 scans at 2 cm^{-1} resolution.

4.2.5   Molecular orbital calculation

In this study, all calculations based on a Dewar and Thief's NDDO (Neglect of Diatomic Different Overlap) approximation were carried out using PM3 method [20] of a semiempirical quantum chemistry program "MOPAC" (Molecular Orbital Package, Fujitsu, SCIGRESS MO Compact 1.0.6 standard) [21-22]. Pople standard template was chosen. The parameter setting is showed in Fig. 4-1.

4.2.6   Gel permeation chromatography (GPC) measurement

Tetrahydrofuran (THF, Wako, dehydrated, no stabilizer) was used as a carrier solvent for gel permeation chromatography (GPC).

4.3   Results and discussion

4.3.1   Optical characterization of Ar plasma jet

4.3.1.1   Typical optical emission spectrum

As is written in chapter 2 and chapter 3, a typical optical emission spectrum of CAPPLAT Ar plasma jet in the wavelength range of 350–950 nm is shown in Fig. 2-8. Emission intensities and assignments of Ar active species (in the wavelength range of 350–950 nm) detected in CAPPLAT

Ar plasma jet are summarized in Table 2-2 [24-28].

When the Ar plasma is generated, the following reactions (4) ~ (6) show the emission process of excited Ar atoms.

$$e^* + Ar^0 \rightarrow Ar^m + e \tag{1}$$

$$e^* + Ar^m \rightarrow Ar^*(4p) + e \tag{2}$$

$$Ar^*(4p) \rightarrow Ar^*(4s) + h\nu \tag{3}$$

Where, Ar^0 indicates the ground state of Ar, Ar^m indicates the metastable state of Ar, and Ar^* denotes the excited state of Ar, e^* indicates the excite state of electron.

4.3.1.2   Effect of additive gas (maleic anhydride) on polymerized OES

The OES of the plasma jet with and without monomer feed are shown in Fig. 4-2.

From the Fig. 4-2, the emission lines from the excited species do not seem to be changed even when the MA monomer was introduced. However, it became weaker when the monomer was introduced. This can be interpreted as the result of the energy transfer from the excited Ar to the MA monomer, which was shown below.

$$Ar^m + M \rightarrow Ar^0 + M^* \tag{4}$$

4.3.1.3   Effect of voltage on polymerized OES

The OES of the plasma jet with MA monomer by changing the voltage is shown in Fig. 4-3. From the Fig. 4-3, the emission lines from the excited species do not seem to be changed even when the voltage was increased. But, it became stronger by increasing the voltage. These results are consistent with the electrical characterization in section 3.2.3 of chapter 3.

4.3.1.4   Effect of additive gas flow rate on polymerized OES

The OES of the plasma jet with MA monomer by changing the carrier gas flow rate is shown in Fig. 4-4. And the contrast of Ar luminescent intensity at 769nm was showed in Fig. 4-5, which

is proved that the Ar metastable energy transferred to the induced monomer through the capillary.

4.3.2 Chemical Structure of the Plasma-Polymerized Films by FT-IR

4.3.2.1 Plasma-polymerized films by FT-IR

By means of theory calculation above, it is possible to deposite the MA monomer by Ar plasma. Now, I analyzed the deposition film by MA monomer through the FT-IR spectra shown in Fig. 4-6 with comparing the MA monomer itself. The value of the monomer feed ratio is expressed as the amount of monomer introduced to the plasma jet per minute.

It is confirmed that MA has been polymerized with keeping its primary structure since the characteristic peaks of C=O (1781 cm^{-1}), C=O (1851 cm^{-1}) in the monomer have been maintained and the peak of C-O-C (1067 cm^{-1} and 1240 cm^{-1}) was observed. Relative to the monomer itself, the intensity of the functional group peak decreased after polymerization. And lacking off the drying treatment after plasma polymerization, the peaks of OH (around 3500cm^{-1}) were appeared. The peak of C=C (1642 cm^{-1}) bond in the monomer disappeared. It is confirmed that the additional polymerization proceeded.

The polymerization result of MA accorded with the calculation result of molecular orbital. It is confirmed that only the C=C bond opened, and the primary structure of the MA monomer was maintained by Ar plasma.

4.3.2.2 Effect of voltage on plasma-polymerized films by FT-IR

The polymeric IR spectrum of MA with changing applied voltage was showed in Fig. 4-7, which has the same tendency as changing the carrier gas flow rate. Although the voltage was increased, the structure of polymerized film was not changed. The peak of C=C (1642 cm^{-1}) bond in all of the polymerized films disappeared. The characteristic peaks of C=O (1781 cm^{-1}), C=O

(1851 cm^{-1}) in the MA monomer have been maintained and the peak of C-O-C (1067 cm^{-1} and 1240 cm^{-1}) were also kept.

Therefore, the results shown in Fig. 4-7 indicate the deposition rate increased as the applied voltage increased and the primary structure was retained, too.

4.3.2.3   Effect of monomer flow rate on plasma-polymerized films by FT-IR

The polymeric IR spectrum of MA with changing flow rate was shown in Fig. 4-8.

The structure of the product did not change even when adjusting the carrier gas rate. The difference in absorption intensity could be attributed to the difference in the thickness of films. The larger monomer feed ratio will lead to the faster deposition rate as well if the plasma intensity is sufficient for the polymerization of the introduced monomer. The results shown in Fig.4-8 indicate the deposition rate increased as the monomer feed ratio increased.

In spite of changing the carrier gas rate, it is also confirmed that primary structure was maintained.

4.3.3   Molecular orbital calculation

The two particular orbitals, which act as the essential part in a wide range of chemical reactions of various compounds, were referred to under the general term of "frontier orbitals", and abbreviated frequently by HOMO (highest occupied molecular orbital) and LUMO (lowest unoccupied molecular orbital) of the S_0 state and singly occupied molecular orbital (SOMO and SOMO') at the singlet excited state (S_1) [23], which is shown in Table 4-2.

According to the calculated eigenvector in the Table 4-2 and the structure of MA in Table 4-1, whatever at ground state or the excited state, the electron density of C (3) and C (5) are lowest. This is the affection of the O atom around. At ground state, the electron density of O (6) and O (7)

are highest of all. The electron density is higher on C (1) and C (2) than any other atom at S_1 state and T_1 state, which suggesting the ionization reaction is almost happened on C=C bond by π- π^* transition. The excited molecule has a characteristics of biradical, and the energy difference between SOMO' and LUMO of ground state is much small (nearly 3.20eV). So their orbital overlap would occur to form a dimmer biradical, which is the reaction (1). The polymerization is thought to be proceeded by polycondensation of the radicals.

$$M^* + M \rightarrow \cdot M\text{-}M\cdot \tag{5}$$

4.3.4 The molecule weight distribution of MA monomer and polymerized film

Molecular weight (Mw) was measured by gel permeation chromatography (GPC) using a column of TOSOH Corporation, TSK gel GMHHR-M with THF as eluent at a flow rate of 1.0 mL/min employing a differential refractometer (TOSOH RI-8020). The calibration curves for GPC analysis were obtained using five linear polystyrene samples ($4.74 \times 10^2 - 7.75 \times 10^5$, Mw / Mn = 1.01−1.2). Therefore, the molecular weights were expressed as the polystyrene equivalent molecular weights.
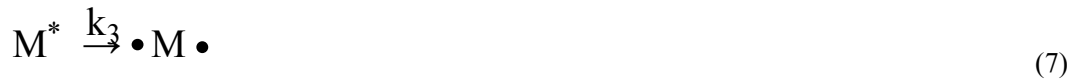
The molecule weight distribution of MA monomer and polymerized MA film was shown in Fig. 4-9. As is shown in the Fig. 4-9, the number-average molecular weight (M_n) of polyMA chains ranged from 170 ~1000. As the MA monomer appeared around log M = 1.9, the peak at log M = 2.24 (the molecular weight is equal to ca. 170) seems the dimmer of MA. The peaks at 2.68 and 3.00 are also supposed to be the hexamer and dodecamer of MA, respectively. The larger molecules are also recognized. It should be noted here that the oligomers of MA observed are of the even number combinations of MA monomer.

4.3.5 Plasma polymerization mechanism

Ar plasma generates many species: ions (Ar^0, Ar^+, Ar^{2+}, and Ar^m), electrons (e), neutrals and so on. Generally, Ar^m contains $^3P_0$ for 11.72eV and $^3P_2$ for 11.55eV [29]. Mostly, Ar^m contains $^3P_0$ for 11.72 eV and $^3P_2$ for 11.55 eV. Ar^m ($^3P_2$) of which excitation energy is 11.55 eV plays an important role since the lifetime of $^3P_2$ is 38 s and longer than that of $^3P_0$, 1.3 s [30]. Therefore, Ar^m ($^3P_2$, 11.55 eV) plays an important role in the Ar plasma.

As the monomer was introduced, Ar plasma emission intensities decreased. And combing the reaction (4), the quantity of Ar metastable will decrease. Consequently, the emission intensities of excited Ar atoms weakened since the reaction (2) was restrained.

On the other hand, as described in section 3.2.5 of chapter 3, when it begins to polymerized, reaction (7) to reaction (9) are also supposed to be happened：

$$M^* + M \xrightarrow{k_1} \bullet M\text{—}M\bullet, \tag{5}$$

$$M^* + M^* \xrightarrow{k_2} \bullet M\text{—}M\bullet \tag{6}$$

$$M^* \xrightarrow{k_3} \bullet M \bullet \tag{7}$$

Here，M^* is the excited state of monomer, $\bullet M\bullet$ is the biradical of the monomer, k is the speed ration. The speed of polymerization is proportion to $k[M^*][M]$ by reaction (5), $k[M^*]^2$ by reaction (6) and $k[M^*]$ by reaction (7) respectively.

And, I assume that the variation of emission density by Ar ($\triangle I$) is proportion to the production of the monomer metastable state. Then I think that the rate of polymerization is proportion to the multiply of $\triangle I$ and monomer concentration by reaction (5), $\triangle I^2$ by reaction (6) and $\triangle I$ by reaction (7) respectively.

The observed results are illustrated in Fig. 4-10. Judging from the R^2 value of the regression line, it was thought that the reaction (5) will be the main polymerization path, which is consistent

with the results of molecular weight distribution of MA and MOPAC calculation.

4.4   Conclusions

In this chapter, the non-equilibrium atmospheric pressure Ar plasma was applied to the polymerization of maleic anhydride (MA). Since the ionization energy of MA is 10.5 eV that is close to the energy of Ar^m, the polymerization mechanism assumed in the former chapters suggested it possible for MA to be polymerized. The intensity of optical emission spectroscopy (OES) of the plasma jet was found to become weaker when the MA monomer was introduced into the jet. This was interpreted as the result of the energy transfer from Ar^m to the monomer. The deposited films were analyzed by using Fourier transform infrared spectroscopy (FT-IR) proving the monomer was successfully polymerized with retaining the functional groups.

It was suggested that the excited MA changed into π-π* transition state to produce dimer biradicals which initiated the polymerization. Through the GPC measurement, it was confirmed that after polymerization MA monomer intensity peak was disappeared and even number combination (dimmer, hexamer and dodecamer) intensity peak were generated, which certify the dimer biradical were produced.

The polymerization kinetics was also used to prove the generated possibility of dimmer biradical, which consistent with the proposal above. So in case of MA, the excited monomers generate dimer biradicals followed by polycondensation with maintaining the primary structure.

References

[1] J. McMurry, Organic Chemistry, Brooks/ Cole: Pacific Grove, CA, 468 (1988).

[2] J. March, Advanced Organic Chemistry, 4th, Wiley: New York, 794 (1992).

[3] H. J. F. Angus, D. Bryrce-Smith, Proc. Chem. Soc., 326 (1959).

[4] G. O. Schenck, R. Steinmetz, Tetrahedron Lett, 1 (1960).

[5] E. Grovenstein, D. V. Rao, W. J. Taylor, J. Am. Chem. Soc., 83, 1705 (1961).

[6] J. J. Pellon, N. M. Smyth, R. L. Kugel, W. M. Thomas, J. Appl. Polym. Sci., 10, 421 (1966).

[7] K. W. Suh, J. M. Corbett, J. Appl. Polym. Sci., 12, 2359 (1968).

[8] T. Kokubo, S. Iwatsuki, Y. Yamashita. Makromol, Chem., 123, 256 (1969).

[9] B. Schneier, J. Polym. Sci., B10, 245 (1972).

[10] T. A. DuPlessis, A. Lustigand, E. Greyling, J. Macromol. Sci. Chem., 11, 1015 (1977).

[11] C. Caze, C. Loucheux, J. Macromol. Sci. Chem., A12, 1501 (1978).

[12] Sahu, U. S. Polym. Commun., 24, 61 (1983).

[13] K. Fujimori, W. S. Schiller, I. E. Craven, Makromol. Chem., 192,959 (1991).

[14] B. D. Roover, M. Sclavons, V. Carlier, J. Devaux, R. Legras, A. J. Momtaz, Polym. Sci, Polym. Chem. Ed., 33, 829 (1995).

Bartlett. P. D, Nozaki. K, J. Am. Chem. Soc. 1946, 68, 1495.

[15] J. P. Deng, W. T. Yang, B. Ranby, J. Eur. Polym., 38, 1449 (2002).

[16] S. Schiller, J. Hu, A. T. A. Jenkins, R. B. Timmons, F. S. Sanchez-Estrada, W. Knoll, R. Förch, Chem. Mater., 14, 235-242 (2002).

[17] http://www.chemindustry.com/apps/chemicals

[18] X. Fei, Y. Kondo, X. Qian, S. Kuroda, T. Mori, K. Hosoi, Key Engineering Materials., 596,

65-69 (2014).

[19] J. Yan, Y. Kondo, X. Qian, X. Fei, K. Hosoi, T. Mori, S. Kuroda, Applied Mechanics and Materials., 423-426, 537-540 (2013).

[20] J.J.P. Stewart, Journal of Computer-Aided Molecular Design., 4(1), 1-103 (1990).

[21] R. M. Metzger, Acc. Chem. Res., 32(11), 950-957 (1999).

[22] SCIGRESS Mo Compact 1.0 User Guide.

[23] Brian. W. C, Theor. Chim. Acta., 87, 415-430 (1994).

[24] Q. S. Yu, H. K. Yasuda, Plasma Chem. Plasma Process., 18, 461 (1998).

[25] M.C. García, M. Varo, P. Martínez, Plasma Chem. Plasma Process., 30, 241 (2010).

[26] A. F. Bublievskii, A. A. Galinovskii, A. V. Gorbunov, S. A. Zhdanok, V. A. Koval, L. I. Sharakhovskii, G. V. Dolgolenko, D. S. Skomorokhov, J. Eng. Phys. Thermophys. 79, 629 (2006).

[27] V. Poenariu, M. R. Wertheimer, R. Bartnikas, Plasma Process. Polym., 3, 17 (2006).

[28] J. Kuba, L. Kucera, F. Plzak, M. Dvorak, J. Mraz, Coincidence Tables for Atomic Spectroscopy, Elsevier Publishing Company (1965).

[29] Y. Harada, S. Masuda, H. Ozaki: Chem. Rev., 97, 1897-1952 (1997).

[30] Y. K. Lee, K. T. Hwang, M. H. Lee and C. W. Chung, J. Korean Phys. Soc. 52 (6), 1792 (2008).

Table 4-1 The properties of polymerized monomer list

Monomer	Molecular Formular	Chemical Formular	Molecular Weight (g/mol)	Density (g/cm^3)	Boiling Point (℃)
Maleic Anhydrides (MA)	$C_4H_2O_3$		98.06	1.314	202

Table 4-2 Electron structure of MA in the ground state and the excited state by PM3

calculation method

| State		S_0		S_1		T_1	
FMO		HOMO	LUMO	SOMO	SOMO'	SOMO	SOMO'
E/eV		-11.7080	-1.5480	-8.7520	-4.7440	-8.1340	-5.2220
	2S	-0.0720	0.0000	0.0000	0.0000	0.0000	0.0000
C(1)	2Px	0.0202	0.0000	0.0000	0.0000	0.0000	0.0000
	2Py	-0.2064	0.0000	0.0000	0.0000	0.0000	0.0000
	2Pz	0.0001	0.5566	0.6473	0.6129	-0.6527	0.6220
Electron Density		0.0482	0.3098	0.4190	0.3756	0.4260	0.3869
	2S	0.0720	0.0000	0.0000	0.0000	0.0000	0.0000
C(2)	2Px	0.0202	0.0000	0.0000	0.0000	0.0000	0.0000
	2Py	0.2064	0.0000	0.0000	0.0000	0.0000	0.0000
	2Pz	0.0000	-0.5566	0.6473	-0.6129	-0.6527	-0.6219
Electron Density		0.0482	0.3098	0.4190	0.3756	0.4260	0.3868
	2S	0.0548	0.0000	0.0000	0.0000	0.0000	0.0000
C(3)	2Px	0.0127	0.0000	0.0000	0.0000	0.0000	0.0000
	2Py	-0.1009	0.0000	0.0000	0.0000	0.0000	0.0000
	2Pz	0.0000	-0.3092	-0.0126	-0.2102	-0.0153	-0.1815
Electron Density		0.0133	0.0956	0.0002	0.0442	0.0002	0.0329
	2S	0.0000	0.0000	0.0000	0.0000	0.0000	0.0000
O(4)	2Px	-0.3443	0.0000	0.0000	0.0000	0.0000	0.0000
	2Py	0.0000	0.0000	0.0000	0.0000	0.0000	0.0000
	2Pz	0.0000	0.0000	-0.0413	0.0000	0.0867	0.0000
Electron Density		0.1185	0.0000	0.0017	0.0000	0.0075	0.0000
	2S	-0.0548	0.0000	0.0000	0.0000	0.0000	0.0000
C(5)	2Px	0.0127	0.0000	0.0000	0.0000	0.0000	0.0000
	2Py	0.1009	0.0000	0.0000	0.0000	0.0000	0.0000
	2Pz	0.0000	0.3092	-0.0126	0.2103	-0.0153	0.1815
Electron Density		0.0133	0.0956	0.0002	0.0442	0.0002	0.0329
	2S	0.0018	0.0000	0.0000	0.0000	0.0000	0.0000
O(6)	2Px	-0.2998	0.0000	0.0000	0.0000	0.0000	0.0000
	2Py	-0.5260	0.0000	0.0000	0.0000	0.0000	0.0000
	2Pz	-0.0001	-0.3076	-0.2828	-0.2830	0.2646	-0.2833
Electron Density		0.3666	0.0946	0.0800	0.0801	0.0700	0.0803
	2S	-0.0018	0.0000	0.0000	0.0000	0.0000	0.0000
O(7)	2Px	-0.2998	0.0000	0.0000	0.0000	0.0000	0.0000
	2Py	0.5261	0.0000	0.0000	0.0000	0.0000	0.0000
	2Pz	0.0000	0.3076	-0.2828	0.2830	0.2646	0.2833
Electron Density		0.3667	0.0946	0.0800	0.0801	0.0700	0.0803
H(8)	1S	0.1124	0.0000	0.0000	0.0000	0.0000	0.0000
H(9)	1S	-0.1124	0.0000	0.0000	0.0000	0.0000	0.0000
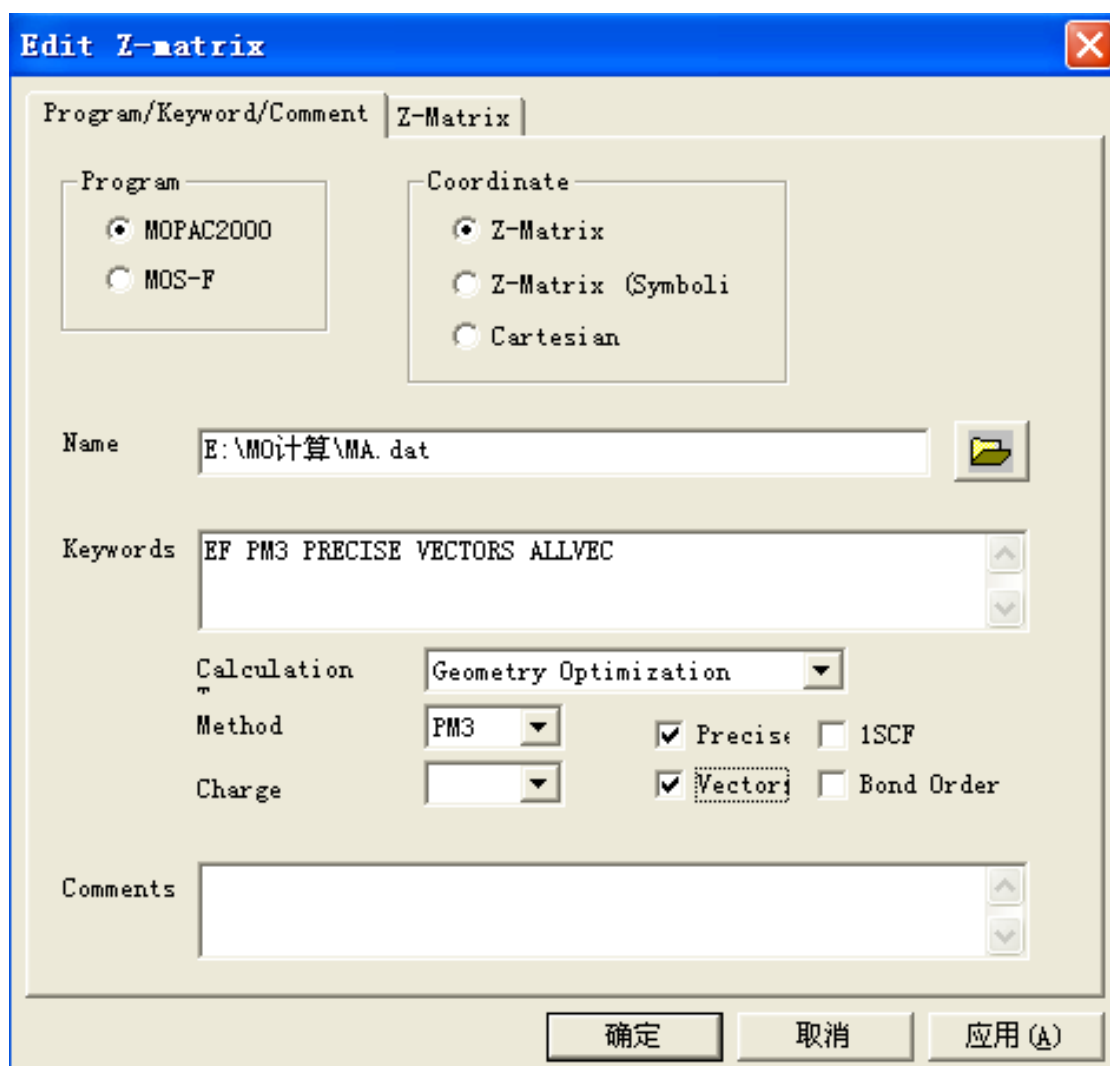
Fig. 4-1 Parameter Setting of MOPAC molecular orbital calculation
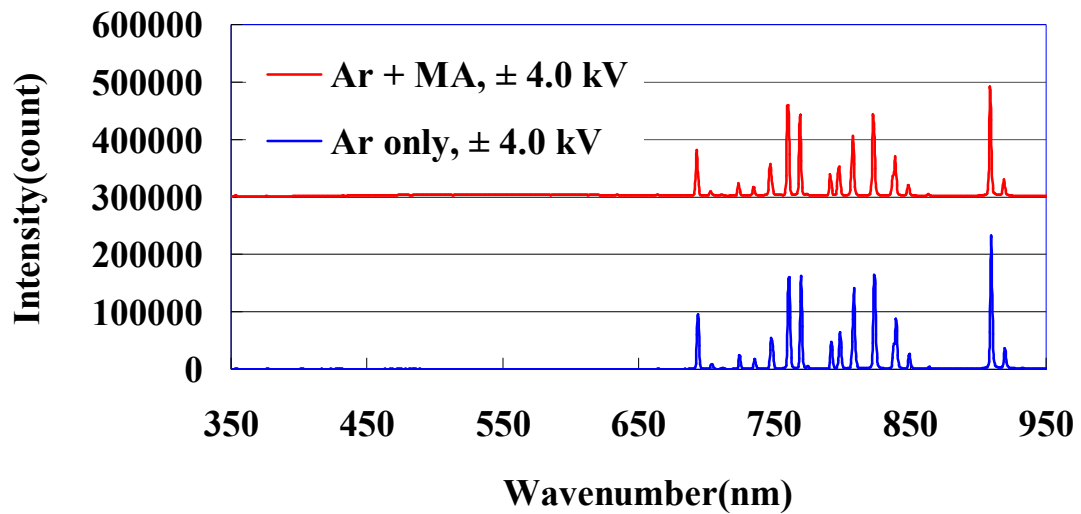
Fig. 4-2 Optical emission spectra of plasma jet with and without MA monomer measured at a distance of 5 mm from the end of torch. Discharge conditions: pure Ar discharge at a flow rate of 3 LPM, carrier gas flow 0.5 L/min, dielectric thickness of 2 mm, nominal applied voltage of ± 4.0 kV (peak to peak) with 50% duty cycle, discharge frequency of 20 kHz.
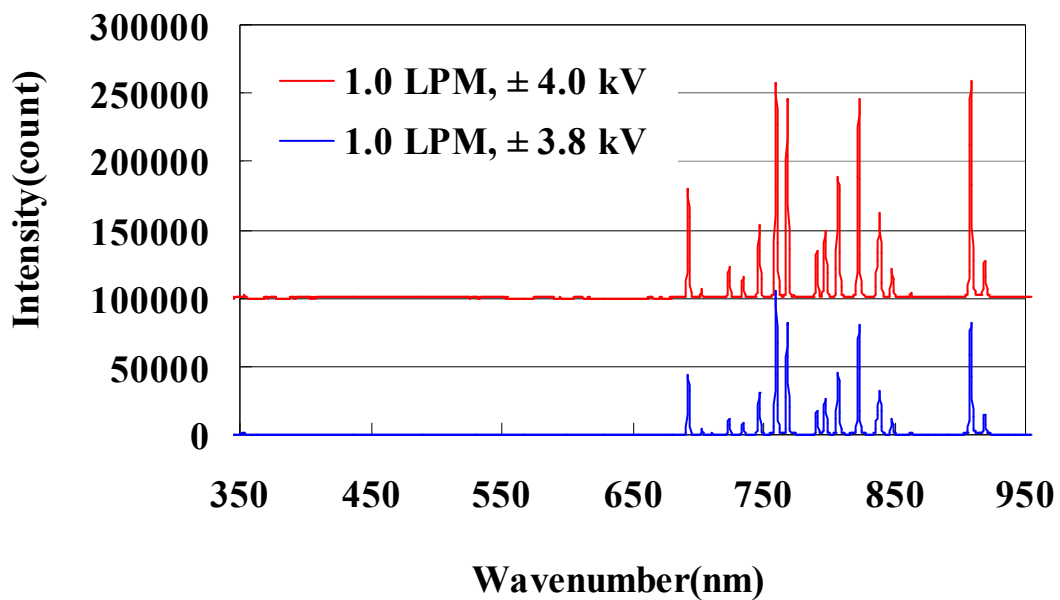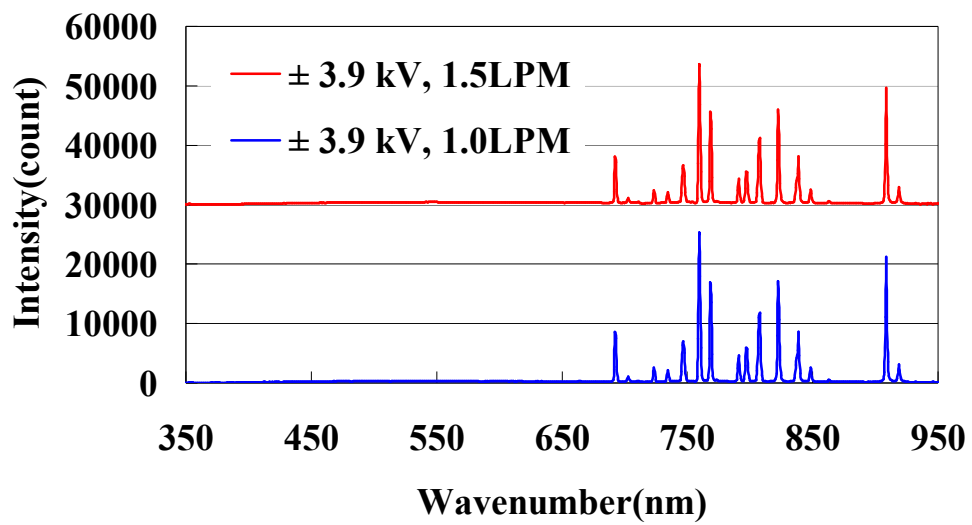
**Fig. 4-3 Optical emission spectra of plasma jet with MA monomer at different voltage measured at a distance of 5 mm from the end of torch. Discharge conditions: pure Ar discharge at a flow rate of 3 LPM, carrier gas flow 1.0 L/min, dielectric thickness of 2 mm, nominal applied voltage of ± 3.8 kV and ± 4.0 kV (peak to peak) with 50% duty cycle, discharge frequency of 20 kHz.**

Fig. 4-4 Optical emission spectra of plasma jet with MA monomer at different carrier gas flow measured at a distance of 5 mm from the end of torch. Discharge conditions: pure Ar discharge at a flow rate of 3 LPM, carrier gas flow 1.0 L/min and 1.5 L/min, dielectric thickness of 2 mm, nominal applied voltage of ± 3.9 kV (peak to peak) with 50% duty cycle, discharge frequency of 20 kHz.
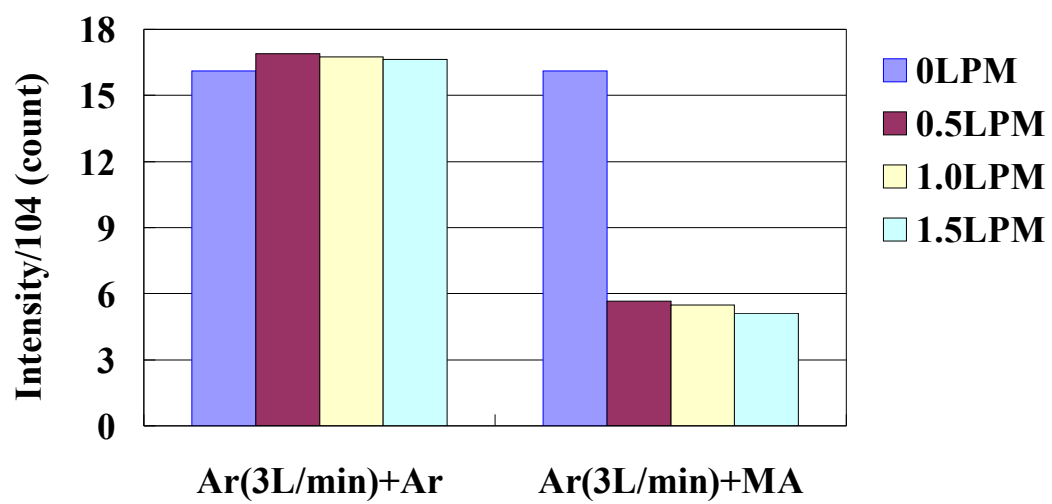
Fig. 4-5 Luminescent intensity of Ar (769nm) luminescent species.
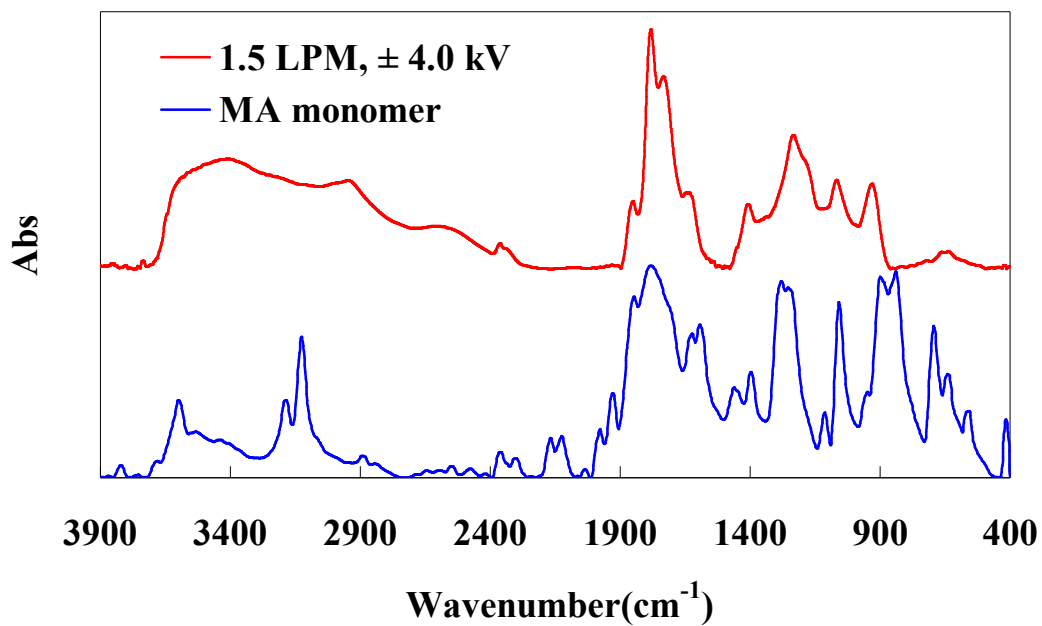
Fig. 4-6 The FT-IR spectrums of MA film and polymerized MA monomer. Discharge conditions: pure Ar discharge at a flow rate of 3 LPM, carrier gas 1.5 LPM, dielectric thickness of 2 mm, nominal applied voltage of ± 4.0 kV (peak to peak) with 50% duty cycle, discharge frequency of 20 kHz.
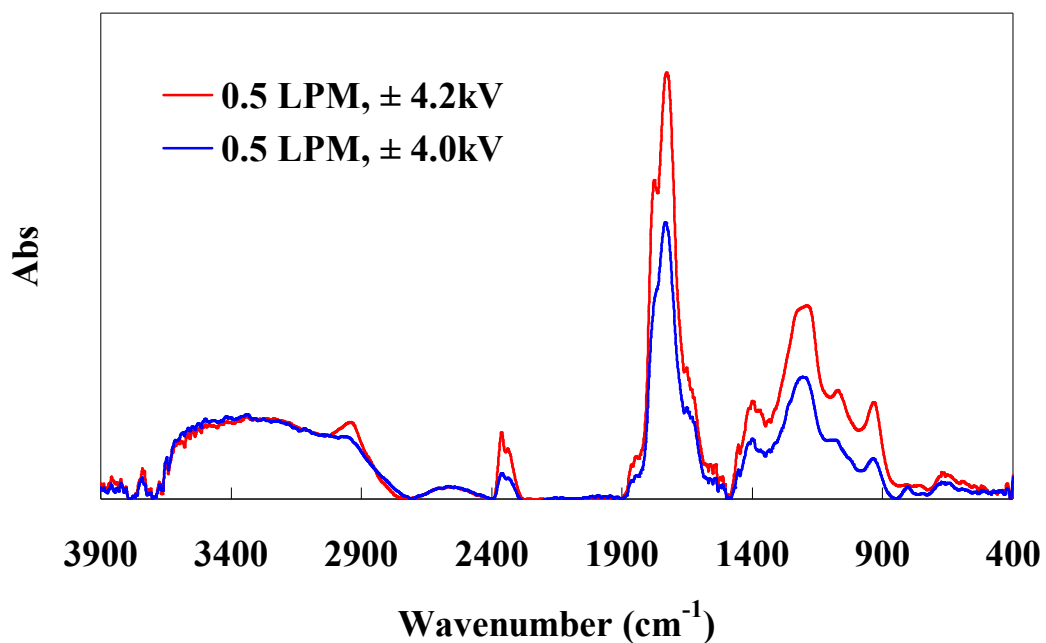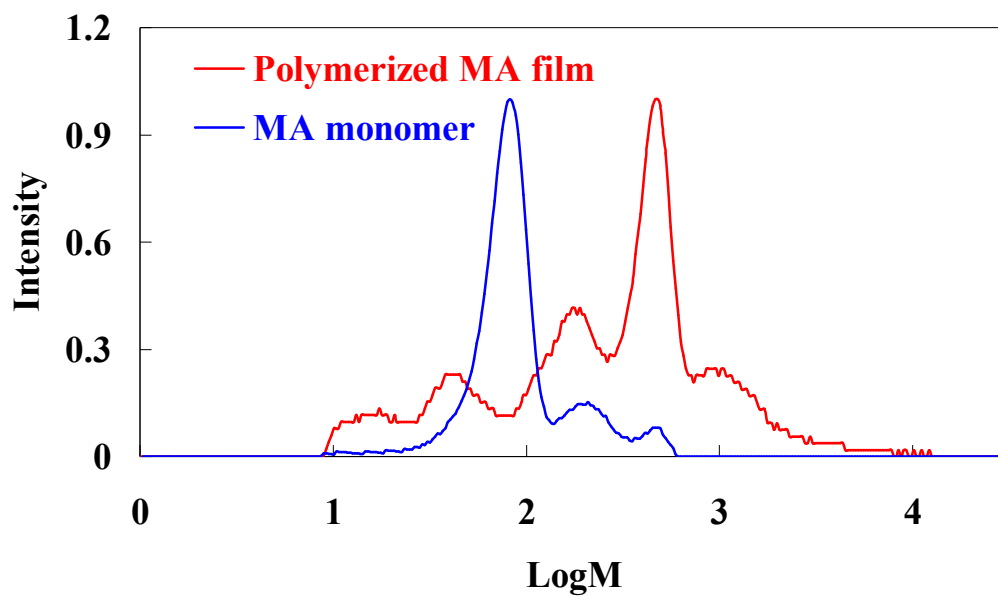
Fig. 4-7 The polymeric IR spectrum of maleic anhydride film by changing the voltage. Discharge conditions: pure Ar discharge at a flow rate of 3 L/min, carrier gas 0.5 L/min，dielectric thickness of 2 mm, nominal applied voltage of ± 4.0 kV and ± 4.2 kV (peak to peak) with 50% duty cycle, discharge frequency of 20 kHz.
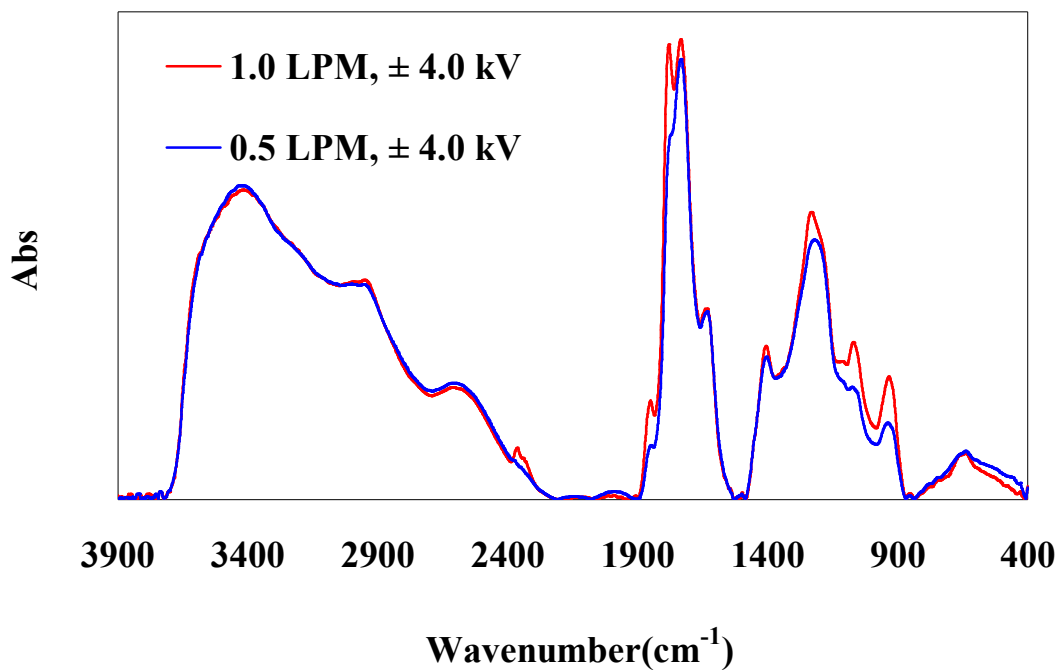
Fig. 4-8 The polymeric IR spectrum of maleic anhydride film by changing the carries gas flow rate. Discharge conditions: pure Ar discharge at a flow rate of 3 LPM, carrier gas 0.5 L/min and 1.0 L/min, dielectric thickness of 2 mm, nominal applied voltage of ± 4.0 kV (peak to peak) with 50% duty cycle, discharge frequency of 20 kHz.

Fig. 4-9 The molecule weight distribution of MA monomer and plasma polymerized MA film.
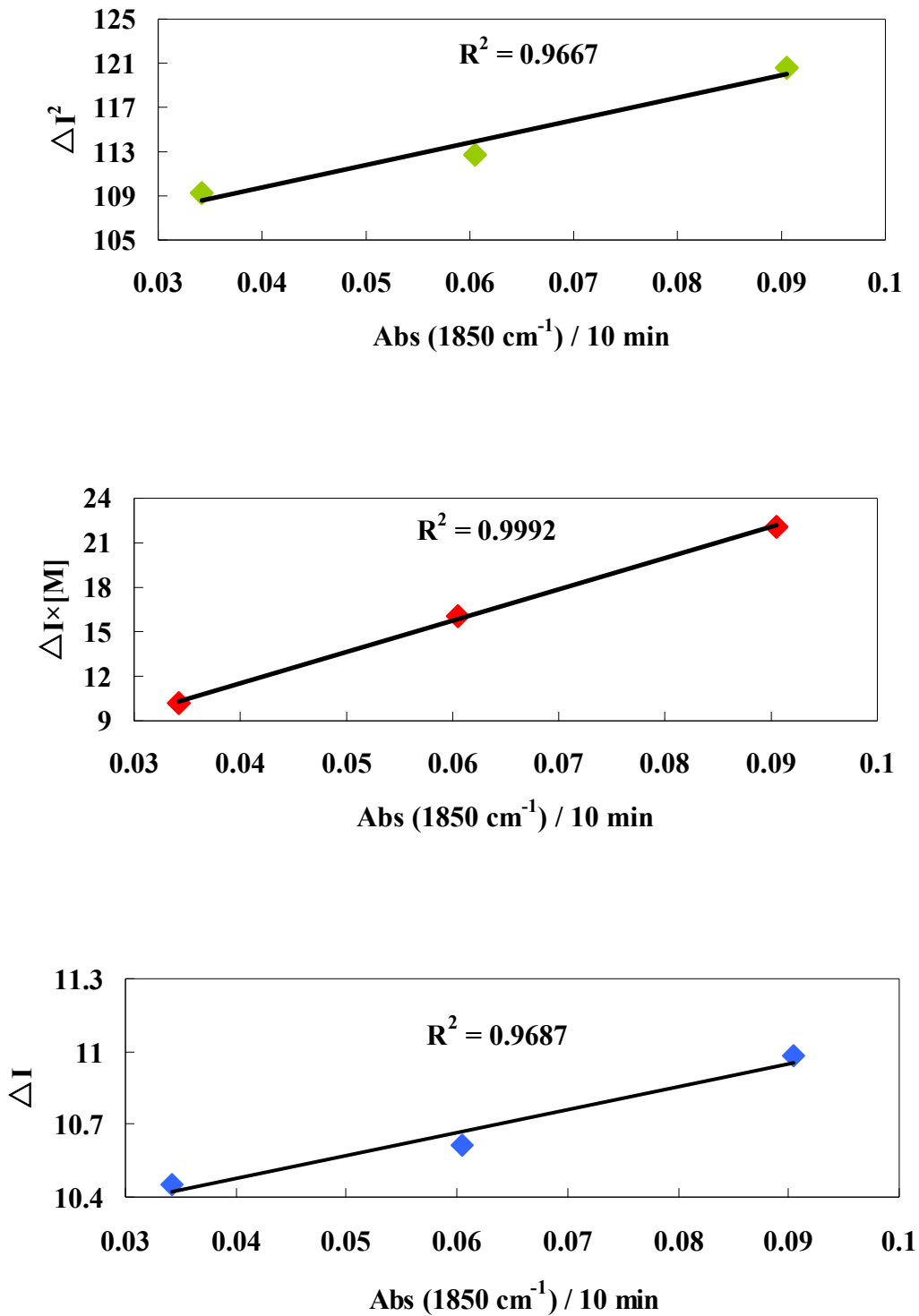
Fig. 4-10 Kinetic analyses of the plasma polymerization of MA. Discharge conditions: pure Ar discharge at a flow rate of 3 L/min, carrier gas 0.5 L/min, 1.0 L/min, 1.5 L/min, dielectric thickness of 2 mm, nominal applied voltage of ± 4.0 kV (peak to peak) with 50% duty cycle, discharge frequency of 20 kHz.

Chapter 5 Summary

Atmospheric pressure non-equilibrium plasma polymerization is a beneficial technology due to its low cost and flexibility in terms of its operation. Though a variety of polymerization have been reported, the polymerization mechanisms induced by the atmospheric pressure plasma are not clear yet, especially on how to maintain the monomer primary structure. In this point of view, it should be remarked that we have succeeded in maintaining the monomer structure through the plasma polymerization of methyl methacrylate (MMA) with using argon (Ar) plasma jet. Thus this thesis aims to clarify the necessary conditions and the mechanism of the polymerization with maintaining the primary structure of monomer induced by the atmospheric pressure non-equilibrium Ar plasma jet. The atmospheric pressure plasma jet was generated by a self-developed plasma device, which has been commercialized under the name of "CAPPLAT" by Cresur Corporation of Japan.

In Chapter 2, in order to explore the conditions for the polymerization MMA was carried out to be polymerized by means of the atmospheric pressure non-equilibrium helium (He) plasma jet. The polymerization using Ar plasma under the same condition was also performed for comparison following Kasih's investigation. The obtained results showed that Ar plasma can polymerize MMA more efficiently than He plasma not only in terms of polymerization rate but also polymer composition. The polymerized MMA by He plasma was recognized to have more disordered structure judging from its broadened C-O-C absorption in Fourier transform infrared (FT-IR) spectrum. This observation brought a working hypothesis that a monomer of which ionization potential is close to or larger than the energy of metastable atom in plasma can be polymerized easily with retaining the primary structure. This working hypothesis was supported by the fact that

styrene of which ionization potential is as small as 8.50 eV, much lower than Ar^m energy, was hardly polymerized by Ar plasma.

In Chapter 3, in order to ascertain the working hypothesis postulated in the former chapter, the non-equilibrium atmospheric pressure plasma was applied for the polymerization of the methacrylic monomers such as (2-hydroxyethyl methacrylate (HEMA), methacrylic acid (MAA) and butyl methacrylate (BMA)). These monomers were selected on the basis of their ionization potential, which was the same to the absolute value of highest occupied molecular orbital (HOMO) calculated results using the PM3 method. It was shown that the selected monomers were successfully polymerized with retaining the functional groups of ester or acid. The polymerization mechanism was discussed on the basis of the optical emission spectroscopy (OES) of the plasma. The Stern-Volmer plot to express the dependency of emission intensity of Ar plasma jet on the monomer concentration became linear indicating that the energy transfer form Ar^m to the monomer took place quantitatively. It was strongly suggested that the functional groups composed of monomer could be retained when the polymerization was proceeded for the monomer of which ionization potential is close to the energy of Ar^m.

In Chapter 4, after verified the hypothesis mentioned above maleic anhydride (MA) was applied to be polymerized with the non-equilibrium atmospheric pressure Ar plasma. Since the ionization energy of MA is 10.5 eV that is close to the energy of Ar^m, the polymerization mechanism assumed in the former chapters suggested it possible for MA to be polymerized. The deposited films were analyzed by using Fourier transform infrared spectroscopy (FT-IR) proving the monomer was successfully polymerized with retaining the functional groups. The intensity of optical emission spectroscopy (OES) of the plasma jet was found to become weaker when the

monomer was introduced into the jet. This was interpreted as the result of the energy transfer from Ar^m to the monomer. It was suggested that the excited MA changed into π-π* transition state to produce dimer biradicals which initiated the polymerization. As it has been assumed that MA polymerizes with much difficulty because of high steric hindrance resulting from disubstitution and only a few exceptional reports have appeared concerning the photo-homopolymerization of MA, the procedure invented in the present study is a promising practical method for the production of homopolymeric materials of MA.

LIST of PUBLICATIONS

1. Atmospheric Pressure Non-Equilibrium Plasma Deposition with Retention of Functional Group

   Jun Yan, Yuki Kondo, Xiaoyi Qian, Xiaomeng Fei, Katsuhiko Hosoi, Tamio Mori and Shin-ichi Kuroda

   Applied Mechanics and Materials, Vols. 423-426 (2013) pp 537.

   Related to chapter 3

2. Polymerization of Maleic Anhydride Induced by Non-Equilibrium Atmospheric Pressure Argon Plasma

   Jun Yan, Katsuhiko Hosoi and Shin-ichi Kuroda

   Applied Mechanics and Materials, accepted

   Related to chapter 4

ACKNOWLEDGEMENTS